Relativistic meson exchange and isobar currents in electron scattering: Noninteracting Fermi gas analysis

M. J. Dekker* and P. J. Brussaard
R. J. Van de Graaff Laboratory, University of Utrecht, P.O Box 80.000, 3508 TA Utrecht, The Netherlands

J. A. Tjon
Institute for Theoretical Physics, University of Utrecht, P.O Box 80.000, 3508 TA Utrecht, The Netherlands
(Received 22 November 1993)

We study two-body currents in the noninteracting relativistic Fermi gas model. Special emphasis is put on the role of the Δ isobar. Due to a resonance behavior, relativistic two-body isobar currents are found to be important in comparison with experimental data. Real-pion production is studied within the same framework, and the importance and physical implications of the energy dependence of the Δ-isobar decay width are stressed.

PACS number(s): 25.30.Fj, 24.30.−v

I. INTRODUCTION

One of the most fruitful ways to obtain information on the nucleus and its constituents has been (and will be) the scattering of leptons off nuclei (for a recent review see, e.g., [1]). The response of the nucleus in these scattering processes can be formulated in terms of structure functions. The latter are solely determined by the properties of the nucleus and allow for direct and stringent tests of models that describe the physics that is probed in these scattering processes. When the projectile energy becomes comparable to or larger than the nucleon mass, one expects a breakdown of a nonrelativistic treatment. One at least needs a relativistic framework to be able to study, in the kinematic region considered, the limits of validity of the conventional physics in terms of meson and nucleon degrees of freedom. In this paper we develop a systematic and consistent analysis of the contribution of relativistic two-body meson exchange and isobar currents, as well as real-pion production in the framework of the relativistic Fermi gas. The first results of this analysis were presented in [2,3]. There are several motivations for this work. The response of the nucleus in an inclusive electron scattering experiment can be phrased in terms of two structure functions: the longitudinal response function which is essentially determined by the nuclear charge distribution and the transverse response function which is determined by the nuclear current distribution. One of the central goals of intermediate-energy physics is to understand the experimental data for these two structure functions, which became available during the early and mid eighties, *simultaneously*. The experimental data of the transverse response function of nuclei obtained from (inclusive) electron scattering at intermediate energies show a distinct two-peak structure as a function of the energy transferred to the nucleus in the scattering process [4,5]. The first originates from the scattering of a single nucleon, the quasifree scattering process. The second is contributed to the excitation of the first nucleon resonance: the Δ isobar. The region in between these two peaks is called, for obvious reasons, the dip region. The experimentally observed strength in the dip region is large. Theoretical models based on one-body processes only, do not give enough overlap in the dip region to account for the observed strength. It was then postulated that two-body processes play an important role in the dip region. We consider two types of two-body currents. One is a direct consequence of the requirement of current conservation at the level of the nuclear electromagnetic current. This requirement gives rise to π meson exchange currents. Their manifestation has been unambiguously identified in deuteron breakup experiments at threshold [6]. Due to the constraints from current conservation there is little ambiguity in the construction of these currents. The second contribution to the two-body current we consider are the Δ-isobar currents. These are much more model dependent since they are not constrained by current conservation. Since both types of two-body currents have little effect on the nuclear charge distribution, these two-body currents will mainly affect the transverse response function. One can therefore hope to give a substantial contribution to the simultaneous understanding of the two response functions.

A first analysis along these lines was carried out in [7]. Van Orden and Donnelly published an extensive report on these calculations of the contribution of two body-currents in a noninteracting Fermi gas model [8]. Their conclusion was that these processes cannot provide the major part of the strength in the dip region. Their analysis is, however, a nonrelativistic one for they apply a static limit procedure which renders the current operators local. One of our objectives is to study how the latter procedure affects their conclusions. This then leads us to the development of a relativistic formulation of the contributions of two-body currents to the response functions,

*Present address: Philips Research Laboratories, WA-03, Prof. Holstlaan 4, 5656 AA Eindhoven, The Netherlands.

the results of which we study in detail. In [2] we showed that the relativistic analysis gives rise to a resonant behavior of the two-body isobar currents and results in a much better description of the dip region.

More recently, data for the nuclear response at much larger energy and momentum transfer on the order of 1 GeV became available [10]. They supply an excellent testing ground for the model we developed, since one may expect *a priori* a breakdown of the static-limit procedure at this energy scale. At the same time one is approaching the energy region where it becomes interesting to study whether a meson-nucleon based model can still provide satisfactory results.

In order to make a meaningful comparison with the data the quasifree scattering process and the real-pion production through an intermediate Δ isobar are treated in the same relativistic Fermi gas model. Concerning the latter an important consistency question in the treatment of the decay width of Δisobar is addressed.

This paper is organized as follows: In Sec. II we introduce some of the most important concepts we use in this paper. In Secs. III and IV the construction and subsequent evaluation of relativistic two-body currents in the relativistic Fermi gas model is carried out. In Sec. V the static limit (SL) of these two-body current contributions is discussed and in Sec. VI the results of the calculations with the full currents are compared with those of the SL currents with special emphasis on qualitative differences. In Sec. VII the contribution from real-pion production through an intermediate Δ isobar is evaluated together with a discussion of the proper way to account for its decay into a πN final state. Then the combined results are presented and compared with data in Sec. VIII. Finally in Sec. IX the main conclusions of this work are summarized. We discuss a few rather technical issues developed for the work presented in this paper in the appendixes.

II. INCLUSIVE ELECTRON SCATTERING

In the one-photon exchange approximation the cross section of inclusive electron scattering can be written, in the laboratory frame, as[1]

$$\frac{d\sigma}{d\epsilon_2 d\Omega} = \sigma_{\text{Mott}} \left[\left(\frac{q^2}{\mathbf{q}^2} \right)^2 R_L + \left(\frac{-q^2}{2\mathbf{q}^2} + \tan^2 \tfrac{1}{2}\theta \right) R_T \right], \tag{2.1}$$

where σ_{Mott} denotes the cross section for spin-$\frac{1}{2}$ scattering off a structureless target and θ the scattering angle of the electron. The longitudinal response function R_L and the transverse response function R_T are determined by the nuclear current operator J^μ. Phrased in terms of the hadronic response tensor $W^{\mu\nu}$ one has

$$R_L = W^{00}, \tag{2.2}$$

$$R_T = -\left(g_{ij} + \frac{q_i q_j}{\mathbf{q}^2} \right) W^{ij}, \tag{2.3}$$

where the Roman indices run from 1 to 3 and

$$W^{\mu\nu} = V \overline{\sum_i} \sum_f (2\pi)^3 \delta^4(P + q - P') \times \langle f|J^\mu(0)|i\rangle \langle f|J^\nu(0)|i\rangle^*. \tag{2.4}$$

V denotes the quantization volume, $|i\rangle$ the initial state with four-momentum P, $|f\rangle$ the final state with four-momentum P' and q denotes the four-momentum transferred to the hadronic system by the virtual photon. The hadronic tensor $W^{\mu\nu}$ is the central object of theoretical studies related to electron scattering experiments.

There is a way to write $W^{\mu\nu}$ (see e.g., [11]) that allows for an evaluation of $W^{\mu\nu}$ according to the rules of quantum field theory and which will be the starting point of the calculations presented in this paper:

$$W^{\mu\nu} = \frac{V}{\pi} \text{Im} \left(i \int d^4x e^{iq\cdot x} \langle i|T[J^\nu(x) J^\mu(0)]|i\rangle \right), \tag{2.5}$$

where T denotes time ordering. This relates $W^{\mu\nu}$ to the imaginary part of the virtual-photon polarization propagator in the nuclear environment (the forward Compton scattering amplitude). Once the hadronic fields with which the photon field can interact and their mutual interactions are specified via an effective Lagrangian, Eq. (2.5) can be treated with the aid of Feynman diagram perturbation theory. The many-body ground state is then treated as an effective vacuum on which the relevant excitations are built and the (noninteracting) Fermi gas Green function is given by

$$\begin{aligned} G_0(p) &= \frac{\not{p} + M}{p^2 - M^2 + i\epsilon} + 2\pi i(\not{p} + M)\delta(p^2 - M^2) \\ &\quad \times \theta(p_0) n(p) \\ &= G_{0_F} + G_{0_D}, \end{aligned} \tag{2.6}$$

where $n(p)$ is the Fermi distribution function, which for zero temperature and in the nuclear-matter rest frame takes the form $\theta(k_F - |\mathbf{p}|) \equiv \theta^<(\mathbf{p})$. For later use we also introduce $\theta^>(\mathbf{p}) \equiv \theta(|\mathbf{p}| - k_F)$. Equation (2.6) defines G_{0_F}, the usual Feynman propagator in vacuum and G_{0_D}, the density-dependent part, which vanishes in the limit of zero density ($k_F \to 0$).

To gain better insight into the physical content of the propagator of Eq. (2.6) we write it in terms of the projection operators onto positive- and negative-energy states:

$$\Lambda^+(\mathbf{p}) = \frac{\hat{\not{p}} + M}{2M} \tag{2.7}$$

and

$$\Lambda^-(\mathbf{p}) = \frac{-\hat{\not{p}} + M}{2M}, \tag{2.8}$$

respectively. Using

$$\not{p} + M = \frac{M}{E_{\mathbf{p}}} ((p_0 + E_{\mathbf{p}})\Lambda^+(\mathbf{p}) - (p_0 - E_{\mathbf{p}})\Lambda^-(-\mathbf{p}))$$

[1] Throughout this paper we use conventions as in Björken and Drell [9].

and

$$2\pi i\delta(p_0 - E_{\mathbf{p}}) = \frac{1}{p_0 - E_{\mathbf{p}} - i\epsilon} - \frac{1}{p_0 - E_{\mathbf{p}} + i\epsilon}$$

we can rewrite Eq. (2.6) as

$$G_0(p) = \frac{M}{E_{\mathbf{p}}}\left[\Lambda^+(\mathbf{p})\left(\frac{\theta^>(\mathbf{p})}{p_0 - E_{\mathbf{p}} + i\epsilon} + \frac{\theta^<(\mathbf{p})}{p_0 - E_{\mathbf{p}} - i\epsilon}\right) - \Lambda^-(-\mathbf{p})\frac{1}{p_0 + E_{\mathbf{p}} - i\epsilon}\right]$$
$$= G_{0_P}(p) + G_{0_H}(p) + G_{0_-}(p), \tag{2.9}$$

where the first term describes the propagation of particles above the Fermi surface the second the propagation of holes below the Fermi surface, and the third the propagation of antiparticles both above and below the Fermi surface.

The approximation to describe the nucleus as a noninteracting infinite system (the free Fermi gas model) deserves more discussion. The justification of this approximation can only be given *a posteriori*. For low energy and momentum transfer this approximation is certainly not valid. Here the effects of the shell structure of the nucleus are extremely important. At energy and momentum transfer between approximately 0.1–1 GeV, there is much circumstantial evidence that this approximation makes sense and that the finite size of the nucleus does not play an essential role. The latter means that the plane wave representation of the wave function is reasonable. The finite size (the decreasing baryon density at the surface) can then be accounted for by the application of the local density approximation. Interactions between the nucleons can be incorporated in a mean-field sense in the nucleon propagator. The power of the present method to evaluate the nuclear response tensor is that it is formulated in terms of (covariant) Green functions, and as such it is suited to incorporate these mean-field interactions in a transparent way.

III. TWO-BODY CURRENTS

In this section we will discuss the construction and subsequent evaluation of two-body currents in the noninteracting Fermi gas model. At the very start of this section we establish what we mean by two-body currents. We consider two types of two-body currents. The first are of mesonic origin, which we will refer to as meson exchange currents (MECs). The second are two-body currents that involve the Δ resonance, often called isobar currents (ICs). When we refer to both at the same time, we simply call them two-body currents.

The essence of the existence of two-body currents is to be found in the conservation of the nuclear current:

$$q_\mu J^\mu = 0. \tag{3.1}$$

In a relativistic field theory this equation states that the coupling of the photon field should preserve the local U(1) gauge invariance present in the free theory. It is beyond the scope of this paper to give a full account of the consequences of this demand in the field of nuclear physics. In particular we will discard the important consistency relation between the two-body interaction and two-body currents, which is allowed as a consequence of the (noninteracting) Fermi gas approximation, and proceed to derive the two-body currents of our interest. For clarity we leave out all form factors in this section. An extensive discussion of form factors can be found in Appendix A.

A. Construction

We start by deriving the lowest-order pionic MECs. Without doubt these are the best established MECs whose form, apart from form factor ambiguities (to be discussed in Appendix A), is the same for many different models and approaches.

As our starting point we take the pseudovector πN Lagrangian:

$$\mathcal{L} = \bar{\psi}_N(i\partial\!\!\!/ - M)\psi_N + \tfrac{1}{2}(\partial_\mu\boldsymbol{\phi}\cdot\partial^\mu\boldsymbol{\phi} - m_\pi^2\boldsymbol{\phi}\cdot\boldsymbol{\phi}) + \frac{g_\pi}{2M}\bar{\psi}_N\, i\partial\!\!\!/\boldsymbol{\phi}\gamma^5\psi_N\cdot\boldsymbol{\tau}, \tag{3.2}$$

where τ denotes the Pauli isospin matrices. Minimal substitution $\partial_\mu \to \partial_\mu + ieA_\mu$ (i.e., $p_\mu \to p_\mu - eA_\mu$) for the charged components of the pion field leads to the interaction vertices with which the currents of Fig. 1 are constructed. To shorten notation we define

$$\Pi(k) = \frac{k\!\!\!/\gamma^5}{k^2 - m_\pi^2}.$$

This leads to the following expressions:

$$J^\mu_{\text{in-flight}} = i(\boldsymbol{\tau}_{(1)}\times\boldsymbol{\tau}_{(2)})^3\left(\frac{g_\pi}{2M}\right)^2\Pi(k_1)_{(1)} \times\Pi(k_2)_{(2)}(k_2 - k_1)^\mu, \tag{3.3}$$

$$J^\mu_{\text{contact}} = i(\boldsymbol{\tau}_{(1)}\times\boldsymbol{\tau}_{(2)})^3\left(\frac{g_\pi}{2M}\right)^2 \times\left[\Pi(k_2)_{(2)}(\gamma^\mu\gamma^5)_{(1)} - \Pi(k_1)_{(1)}(\gamma^\mu\gamma^5)_{(2)}\right]. \tag{3.4}$$

Rather trivially these currents are what we call relativistic MECs.

As mentioned before, the Δ isobar plays a crucial role in the understanding of the nuclear response functions

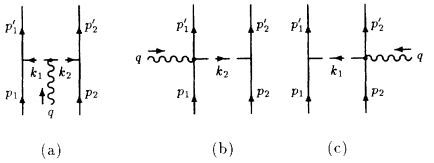

FIG. 1. The Feynman diagrams representing the pion-exchange current. Diagram (a) will be called the "pion-in-flight current," diagrams (b) and (c) the "contact-current."

in the intermediate-energy region. We now derive the contribution to the two-body current due to the excitation of a Δ isobar in the intermediate state (see the four diagrams in Fig. 2).

First we have to specify an effective Lagrangian that involves interacting pion, nucleon, and Δ fields. In this picture the Δ isobar is treated as a separate degree of freedom, not as a πN resonance. We therefore have to extend the Lagrangian of Eq. (3.2) with a spin- and isospin-$\frac{3}{2}$ field representing the Δ isobar. We use the Lagrangian of Peccei [12], which is based on the Rarita-Schwinger (RS) formalism. The main reason for this choice is that we want to compare the results of this work with that of Van Orden and Donnelly [8] who used Peccei's Lagrangian. Apart from that, the Δ part of this Lagrangian is well suited for our relativistic analysis, since special care is taken of the off-shell extrapolation of the interaction vertices. This guarantees that, also off-shell, only the spin-$\frac{3}{2}$ component of the RS Δ field contributes to the amplitudes. A second important ingredient is chiral symmetry from which the πN sector of the Lagrangian is constructed. The resulting linear πN coupling is of pseudovector type. Since we neglect the nonlinear terms (in the pion field) that arise, the πN sector is already displayed in Eq. (3.2). We now discuss the most important features of the incorporation of the Δ field.

Although there is a general freedom in the expression for the free Δ Lagrangian (see e.g., [12]), due to invariance under transformations that do not have an effect on the spin-$\frac{3}{2}$ part of the field, we will here choose the simplest form possible:

$$\mathcal{L}_\Delta = -\bar{\psi}^\mu_\Delta[(g_{\mu\nu}i\partial\!\!\!/ - \gamma_\nu i\partial_\mu - \gamma_\mu i\partial\!\!\!/\gamma_\nu) - M_\Delta(g_{\mu\nu} - \gamma_\mu\gamma_\nu)]\psi^\nu_\Delta. \tag{3.5}$$

This choice can be considered as choosing a specific gauge for the transformations mentioned above. One then has the RS Δ propagator:

$$G^{\mu\nu}_\Delta(p) = \frac{p\!\!\!/ + M_\Delta}{p^2 - M^2_\Delta}\left[-g^{\mu\nu} + \tfrac{2}{3}\frac{p^\mu p^\nu}{M^2_\Delta} - \frac{1}{3M_\Delta}(p^\mu\gamma^\nu - p^\nu\gamma^\mu) + \tfrac{1}{3}\gamma^\mu\gamma^\nu\right]. \tag{3.6}$$

There is an ongoing discussion in the literature whether this is a correct way to treat the spin-$\frac{3}{2}$ field. Another frequently used form for the Δ propagator is given by

$$G^{\mu\nu}_\Delta(p) = \frac{p\!\!\!/ + M_\Delta}{p^2 - M^2_\Delta}(P^{\mu\nu})^{3/2} \tag{3.7}$$

with

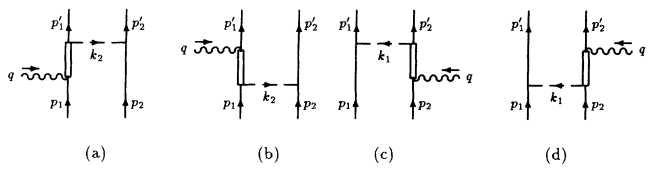

FIG. 2. The Feynman diagrams representing the Δ-isobar current.

$$P^{3/2}_{\mu\nu} = -\left[g_{\mu\nu} - \tfrac{1}{3}\gamma_\mu\gamma_\nu - \frac{1}{3p^2}(p\!\!\!/\gamma_\mu p_\nu + p_\mu\gamma_\nu p\!\!\!/)\right]. \tag{3.8}$$

Comparing these expressions for the propagator, one can show, by commuting $p\!\!\!/$ through γ^ν, that they are only on mass shell ($p^2 = M^2_\Delta$) identical. For a further discussion of their relationship we refer to [13].

Next we discuss the interactions. The interaction vertices $\mathcal{O}^{\mu\nu}$ are restrained by the condition

$$\gamma_\mu\mathcal{O}^{\mu\nu} = 0. \tag{3.9}$$

This is a generalization of the property

$$\gamma_\mu\psi^\mu_\Delta = 0 \tag{3.10}$$

of the on-shell free Δ field, which assures that there is no direct coupling to the spin-$\frac{1}{2}$ component possible [14]. This leads to the $\pi N\Delta$-interaction term:

$$\mathcal{L}_{\pi N\Delta} = \frac{if_{\pi N\Delta}}{m_\pi}\bar{\psi}^\mu_\Delta(4g_{\mu\nu} - \gamma_\mu\gamma_\nu)\mathbf{T}^\dagger\psi_N\partial^\nu\cdot\boldsymbol{\phi} + \text{H.c.}, \tag{3.11}$$

where $\mathbf{T}^\dagger$ represents the 2×4 isospin coupling matrices, which obey the relation

$$T^i(T^\dagger)^j = \delta^{ij} - \tfrac{1}{3}\tau^i\tau^j. \tag{3.12}$$

On shell the $\gamma_\mu\gamma_\nu$ term vanishes and so this term determines the off-shell extrapolation. Defining vertices in Fig. 3, we have the expressions

$$\Delta\to\pi N: \quad \frac{if_{\pi N\Delta}}{m_\pi}k_\nu(4g^{\mu\nu} - \gamma^\nu\gamma^\mu)T^i \equiv \frac{if_{\pi N\Delta}}{m_\pi}k_\nu\mathcal{F}^{\nu\mu}T^i, \tag{3.13}$$

$$\pi N\to\Delta: \quad \frac{-if_{\pi N\Delta}}{m_\pi}\mathcal{F}^{\mu\nu}k_\nu(T^\dagger)^i, \tag{3.14}$$

where the pion momentum k is defined outgoing in both cases. The Roman index i refers to the isospin of the pion. Finally the phenomenological $\gamma N\Delta$ vertex is given by

$$\Delta\to\gamma N: \quad \frac{f_{\gamma N\Delta}}{2M}(q\!\!\!/ g^{\mu\nu} - \gamma^\mu q^\nu - \tfrac{1}{2}iq_\alpha\sigma^{\alpha\mu}\gamma^\nu)\gamma^5T^3 \equiv \frac{f_{\gamma N\Delta}}{2M}G^{\mu\nu}T^3, \tag{3.15}$$

$$\gamma N\to\Delta: \quad \frac{f_{\gamma N\Delta}}{2M}(q\!\!\!/ g^{\mu\nu} - \gamma^\mu q^\nu + \tfrac{1}{2}iq_\alpha\gamma^\nu\sigma^{\alpha\mu})\gamma^5(T^\dagger)^3. \tag{3.16}$$

We are now in a position to write down the expressions for the four diagrams in Fig. 2 containing a Δ isobar in the intermediate state. First the isospin structure for

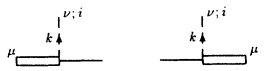

FIG. 3. $\pi N\Delta$ coupling vertices.

diagram (a) in Fig. 2 is given by

$$\mathcal{I} = T^b_{(1)} T^{\dagger 3}_{(1)} \delta^{bc} \tau^c_{(2)}, \tag{3.17}$$

which with the aid of Eq. (3.12) can be written as

$$\mathcal{I} = \tfrac{2}{3}\tau^3_{(2)} - \tfrac{1}{3} i(\boldsymbol{\tau}_{(1)} \times \boldsymbol{\tau}_{(2)})^3. \tag{3.18}$$

For diagram (b) of Fig. 2 we find the isospin factor $\mathcal{I}^\dagger$. A shorthand notation for the isobar current is then given by

$$J^\mu_\Delta = \frac{f_{\pi NN} f_{\gamma N\Delta} f_{\pi N\Delta}}{2M m_\pi^2} \left[\mathcal{I}\, k_{2_\alpha}\, \mathcal{F}^{\alpha\beta} G_{\Delta\beta\delta}(p_1 + q) \mathcal{G}^{\delta\mu} - \mathcal{I}^\dagger \mathcal{G}^{\mu\delta} G_{\Delta\delta\beta}(p_1' - q) \mathcal{F}^{\beta\alpha} k_{2_\alpha} \right] \Pi(k_2)_{(2)} + (1 \leftrightarrow 2)\,, \tag{3.19}$$

where the last term, interchange of the particle labels 1 and 2, represents the contribution of diagrams (c) and (d) of Fig. 2. This current is manifestly conserved (contraction with q^μ gives trivially zero) and is therefore much more model-dependent than the pionic current. It is not the most general Δ current one can consider (see e.g., [15]), but the parts we do not include are in practice much smaller than the transverse part we do include here.

The full two-body current (apart from form factors, see Appendix A) we will consider is given by the sum of the pion currents [Eqs. (3.3) and (3.4)] and Δ-isobar current [Eq. (3.19)]:

$$J^\mu_{\text{full}} = J^\mu_\Delta + J^\mu_{\text{contact}} + J^\mu_{\text{in-flight}}. \tag{3.20}$$

B. The Δ decay width

If the Δ current which we derived in the preceding subsection is applied in the resonance region, the possible decay into a physical πN state should be accounted for. As a consequence the (real) resonance mass M_Δ has to be replaced by $M_\Delta - i\Gamma(s)/2$, where $\Gamma(s)$ denotes the energy-dependent decay width. Since the energy dependence of this width is going to play a crucial role in Sec. VII, we will derive it here, to a large extent along the lines of [16]. The decay width is given by (minus twice) the imaginary part of the Δ self-energy of the diagram in Fig. 4. According to the rules of the previous section, the expression for the self-energy is given by

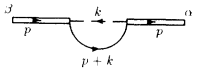

FIG. 4. Δ-isobar self-energy diagram. The imaginary part of this diagram determines the Δ-isobar decay width in vacuum.

$$\frac{\Sigma^{\alpha\beta}_{\pi N}}{i} = (T^\dagger)^a T^a \int \frac{d^4k}{(2\pi)^4} \frac{-i f_{\pi N\Delta}}{m_\pi} (-k_\delta) \mathcal{F}^{\alpha\delta} \times \frac{i}{k^2 - m_\pi^2} \frac{i(\not{q} + M)}{q^2 - M^2} \frac{i f_{\pi N\Delta}}{m_\pi} \mathcal{F}^{\epsilon\beta} k_\epsilon \tag{3.21}$$

with $q = p + k$. Multiplying the isospin factor $(T^\dagger)^a T^a$ from the left with T^b and from the right with $(T^\dagger)^c$ and using Eq. (3.12), one can verify that the isospin operator in Eq. (3.21) equals the identity operator. As is clear from the expression (3.21), this self-energy has a complicated Lorentz structure, which makes it difficult to solve Dyson's equation. Van Faassen [16] argues that all spin-dependent terms vanish on-shell, and that the only remaining Lorentz structure on-shell is given by $g^{\alpha\beta}$. He restricts himself to this term and evaluates the self-energy accordingly. We make an essentially equivalent approximation by sandwiching the self-energy of Eq. (3.21) between RS Δ spinors with invariant mass $\sqrt{s} \equiv W$ for which we generalize the on-shell Rarita-Schwinger spinor sum projection operator to

$$\sum_\sigma u^\mu_\Delta(\sqrt{s}, \sigma) \bar{u}^\nu_\Delta(\sqrt{s}, \sigma) = \frac{\not{p} + \sqrt{s}}{2\sqrt{s}} (P^{\mu\nu})^{3/2}. \tag{3.22}$$

If we now average over spin projections, we have

$$\Sigma_{\pi N}(s) \equiv \tfrac{1}{4} \sum_\sigma \bar{u}^\mu_\Delta(\sqrt{s}, \sigma) \Sigma_{\mu\nu} u^\nu_\Delta(\sqrt{s}, \sigma) \tag{3.23}$$

$$= -i \int \frac{d^4k}{(2\pi)^4} \frac{f^2_{\pi N\Delta}}{2\sqrt{s} m_\pi^2 (q^2 - M^2)(k^2 - m_\pi^2)} \tfrac{1}{4} \mathrm{Tr}[(-k_\alpha) \mathcal{F}^{\mu\alpha} (\not{q} + M) k_\beta \mathcal{F}^{\beta\nu} (\not{p} + \sqrt{s}) P^{3/2}_{\nu\mu}]$$

$$= -i \int \frac{d^4k}{(2\pi)^4} \frac{(4 f_{\pi N\Delta})^2}{8\sqrt{s} m_\pi^2 (q^2 - M^2)(k^2 - m_\pi^2)} \tfrac{1}{3} \left(q^2 - \frac{(q \cdot p)^2}{s} \right) \left(M + \frac{k \cdot p}{\sqrt{s}} \right). \tag{3.24}$$

We evaluate this integral in the frame $\mathbf{p} = 0$, carry out a contour integration over k_0 and define $W_{\mathbf{q}} = E_{\mathbf{q}} + E^\pi_{\mathbf{q}}$ with $E^\pi_{\mathbf{q}} = \sqrt{m_\pi^2 + \mathbf{q}^2}$, and find

$$\Sigma_{\pi N}(s) = \frac{(4 f_{\pi N\Delta})^2}{24 m_\pi^2} \int_0^\infty dq\, q^4 \left(M + \sqrt{s} \frac{E_{\mathbf{q}}}{W_{\mathbf{q}}} \right) \frac{W_{\mathbf{q}}}{2 E_{\mathbf{q}} E^\pi_{\mathbf{q}}} \times \frac{1}{s - W^2_{\mathbf{q}} + i\epsilon}. \tag{3.25}$$

Taking the imaginary part and introducing the decay momentum in the c.m. frame

$$k^2 = \frac{1}{4s} [s - (M + m_\pi)^2][s - (M - m_\pi)^2] \tag{3.26}$$

we obtain the energy-dependent width

$$\Gamma(s) \equiv -2\mathrm{Im}[\Sigma_{\pi N}(s)] = \frac{(4 f_{\pi N\Delta})^2}{12\pi m_\pi^2} \frac{k^3}{\sqrt{s}} (M + E_{\mathbf{k}}). \tag{3.27}$$

The minor differences with the result of Van Faassen vanish at the resonance, as one would expect. The energy dependence of the width effectively accounts for the allowed phase space for the pion produced in the physical decay process. This feature will be explicitly shown in Sec. VII C. From this it follows that at resonance ($\sqrt{s} = 1232$ MeV), with $k = 1.14$ fm^{-1} and experimentally $\Gamma = 115$ MeV, one finds $(4f_{\pi N\Delta})^2/4\pi = 0.38$. We choose to write $4f_{\pi N\Delta}$ since this is the quantity to be compared with the coupling constants used in other works. We thus see that the $\pi N\Delta$ coupling constant is determined by the Δ decay width.

Since, by averaging over spins, we obtain a purely scalar self-energy, it is easy to include it, via Dyson's equation, in the Δ propagator of Eq. (3.7). To this end we note that we have $(P^{3/2})^{\mu\nu}(P^{3/2})_\nu{}^\rho = (P^{3/2})^{\mu\rho}$ and $[\not{p}, (P^{3/2})^{\mu\nu}] = 0$. If one then assumes that the solution to Dyson's equation is of the same operator form as the free propagator, the (exact) solution is simply given by the free one with the replacement of the denominator by: $p^2 - M_\Delta^2 - 2\sqrt{s}\Sigma$. This simply follows by construction since we project in every intermediate state to the pure spin-$\frac{3}{2}$ components of the field. Absorbing the real part in the physical definition of the resonance mass, the appearance of the imaginary part is simulated by the replacement $M_\Delta \to M_\Delta - i\Gamma/2$. This procedure is certainly not exact for the RS Δ propagator of Eq. (3.6). There all off-shell ambiguities are still present. We choose, however, to include the width also in the case of the RS Δ propagator by applying the above-mentioned replacement of the denominator.

IV. EVALUATION OF TWO-PARTICLE–TWO-HOLE CONTRIBUTION TO $W^{\mu\nu}$

Now that we have specified our two-body current in the preceding section, we are in a position to evaluate its contribution to $W^{\mu\nu}$. As long as we neglect the one-particle–one-hole (1p1h) excitations in the nuclear ground state, it is easy to see that only the two-body current can contribute to the 2p2h channel and no interference with the one-body current can occur. Since one can show that the only remaining interference term amounts to a modification of the one-body current due to the interactions in the initial-state wave function we will not consider this contribution in this work. We now evaluate the two-body knockout contribution to $W^{\mu\nu}$:

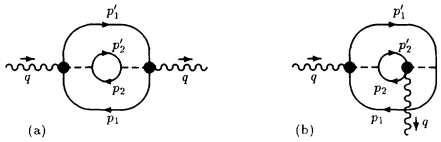

FIG. 5. 2p2h-excitation diagrams. The diagrammatic content of the blobs in these diagrams is given in Fig. 6.

$$W^{\mu\nu}_{\rm 2p2h} = \sum_{\rm 2p2h} \langle {\rm FG}|J^{\dagger\,\nu}_{(2)}|{\rm 2p2h}\rangle\langle {\rm 2p2h}|J^{\mu}_{(2)}|{\rm FG}\rangle, \qquad (4.1)$$

where $|{\rm FG}\rangle$ is the noninteracting Fermi gas ground state. Here we will show how the use of the approach outlined in Sec. II leads to results that allow for an intuitive interpretation: $W^{\mu\nu}$ as a Fermi gas phase-space integral over an elementary scattering amplitude. Furthermore the structure of these results allows the use of Dirac matrix algebra to abandon the static limit. The relevant diagrams are given in Fig. 5. To establish notation, we denote the general $\gamma\pi NN$ vertex by Γ^μ (represented in the figures by the blob which contains the sum of the diagrams in Fig. 6) and the πNN vertex by P. We then have, using Eq. (2.9), for the direct contribution [diagram (a) of Fig. 5]

$$W^{\mu\nu}_{\rm 2p2h} = \frac{1}{\pi} V\ {\rm Im} \sum_{\rm isospin} \int \frac{d^4p_1}{(2\pi)^4}\frac{d^4p_2}{(2\pi)^4}\frac{d^4p_1'}{(2\pi)^4}\frac{d^4p_2'}{(2\pi)^4} {\rm Tr}[\bar{\Gamma}^\nu \Lambda^+(\mathbf{p}_1')\Gamma^\mu\Lambda^+(\mathbf{p}_1)]{\rm Tr}[\overline{P}\Lambda^+(\mathbf{p}_2')P\Lambda^+(\mathbf{p}_2)] \left(\frac{1}{(p_2'-p_2)^2 - m_\pi^2}\right)^2$$
$$\times S(p_1,p_2,p_1',p_2')(2\pi)^4\delta^4(p_1+p_2+q-p_1'-p_2') \qquad (4.2)$$

with

$$S(p_1,p_2,p_1',p_2') = i\frac{M^4}{E_{\mathbf{p}_1}\cdots E_{\mathbf{p}_2'}}[G_{0_P}(p_1)+G_{0_H}(p_1)]\cdots[G_{0_P}(p_2')+G_{0_H}(p_2')]. \qquad (4.3)$$

Equation (4.2) can be simplified if we note that we only need the 2p2h final state contribution of this diagram. Carrying out, in S, the trivial integration over p_2' (to shorten notation we write $\mathbf{p}_2'$ instead of $\mathbf{p}_1+\mathbf{p}_2+\mathbf{q}-\mathbf{p}_1'$, however) and the integrations over p_{1_0}, p_{2_0}, and p_{1_0}', we find

$$\int \frac{dp_{1_0}}{2\pi}\frac{dp_{2_0}}{2\pi}\frac{dp_{1_0}'}{2\pi} S(p_1,p_2,p_1') = \frac{M^4}{E_{\mathbf{p}_1}E_{\mathbf{p}_2}E_{\mathbf{p}_1'}E_{\mathbf{p}_2'}}\theta^<(\mathbf{p}_1)\theta^<(\mathbf{p}_2)\theta^>(\mathbf{p}_1')\theta^>(\mathbf{p}_2')$$
$$\times\left(\frac{1}{E_{\mathbf{p}_1}+E_{\mathbf{p}_2}+q_0-E_{\mathbf{p}_1'}-E_{\mathbf{p}_2'}+i\epsilon}+(q_0\to -q_0)\right). \qquad (4.4)$$

As a result Eq. (4.2) reduces for positive q_0 to

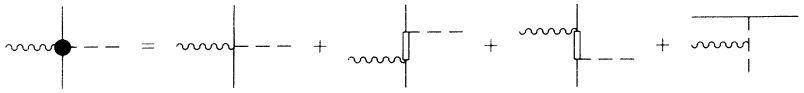

FIG. 6. The diagrammatic content of the blob in Fig. 5.

$$W^{\mu\nu}_{\rm 2p2h} = V \sum_{\rm isospin} \int \frac{d\mathbf{p}_1}{(2\pi)^3} \frac{d\mathbf{p}_2}{(2\pi)^3} \frac{d\mathbf{p}_1'}{(2\pi)^3} \frac{M^4}{E_{\mathbf{p}_1} E_{\mathbf{p}_2} E_{\mathbf{p}_1'} E_{\mathbf{p}_2'}} \theta^<(\mathbf{p}_1)\theta^<(\mathbf{p}_2)\theta^>(\mathbf{p}_1')\theta^>(\mathbf{p}_2') \delta(E_{\mathbf{p}_1} + E_{\mathbf{p}_2} + q_0 - E_{\mathbf{p}_1'} - E_{\mathbf{p}_2'})$$
$$\times \left(\frac{1}{k_2^2 - m_\pi^2} \right)^2 \mathrm{Tr}[\bar{\Gamma}^\nu \Lambda^+(\mathbf{p}_1')\Gamma^\mu \Lambda^+(\mathbf{p}_1)] \, \mathrm{Tr}[\overline{P} \Lambda^+(\mathbf{p}_2') P \Lambda^+(\mathbf{p}_2)]. \tag{4.5}$$

For diagram (b) in Fig. 5 where the photon coupling resides both in particle (spin) lines 1 and 2, a similar procedure can be carried out which gives completely analogous results. The full result can now be written as

$$W^{\mu\nu}_{\rm 2p2h} = \tfrac{1}{2} V \sum_{\rm isospin} \int \frac{d\mathbf{p}_1}{(2\pi)^3} \frac{d\mathbf{p}_2}{(2\pi)^3} \frac{d\mathbf{p}_1'}{(2\pi)^3} \frac{M^4}{E_{\mathbf{p}_1} E_{\mathbf{p}_2} E_{\mathbf{p}_1'} E_{\mathbf{p}_2'}} \theta^<(\mathbf{p}_1)\theta^<(\mathbf{p}_2)\theta^>(\mathbf{p}_1')\theta^>(\mathbf{p}_2') \delta(E_{\mathbf{p}_1} + E_{\mathbf{p}_2} + q_0 - E_{\mathbf{p}_1'} - E_{\mathbf{p}_2'})$$
$$\times \mathrm{Tr}_{1,2}[\bar{J}^\nu_{(2)} \Lambda^+(\mathbf{p}_1')\Lambda^+(\mathbf{p}_2') J^\mu_{(2)} \Lambda^+(\mathbf{p}_1)\Lambda^+(\mathbf{p}_2)], \tag{4.6}$$

where J^μ is given by the sum of both pion and isobar currents, the explicit expression of which can be found in the previous sections. The factor $\frac{1}{2}$ accounts for the double counting that occurs in this notation (two other diagrams, topologically equivalent to the diagrams of Fig. 5, are included in the last expression). The index 1,2 at the trace symbol indicates that for both particle 1 and particle 2 an independent trace is at stake. We may observe that the structure of the result can be interpreted as the product of a Fermi gas phase-space factor times the spin-summed square of the invariant amplitude of an elementary scattering process.

For the crossed (Pauli exchange) contribution (the diagram of Fig. 7), the procedure discussed above leads to an expression similar to Eq. (4.5), where the last line is replaced by

$$\frac{1}{(k_2^2 - m_\pi^2)((p_1' - p_2)^2 - m_\pi^2)} \mathrm{Tr}[\bar{\Gamma}^\nu \Lambda^+(\mathbf{p}_2') P \Lambda^+(\mathbf{p}_2) \overline{P} \Lambda^+(\mathbf{p}_1') \Gamma^\mu \Lambda^+(\mathbf{p}_1)].$$

Furthermore, due to the fact that only one, instead of two (in the case of the direct term) closed fermion loops are present it gets a relative minus sign, compared to the direct contribution. We see that only a single trace occurs. This single trace happens to be in practice too cumbersome to handle for the isobar currents. In that case we resort to the derivation in the second-quantization scheme. There the spin summations are transformed to projection operators, such that the resulting expression for the direct contribution is exactly equal to the one we derived here. For the exchange term this procedure is more involved and for details we refer to Appendix B. The final result can now be summarized:

$$W^{\mu\nu}_{\rm 2p2h} = \tfrac{1}{2} V \sum_{\rm isospin} \int \frac{d\mathbf{p}_1}{(2\pi)^3} \frac{d\mathbf{p}_2}{(2\pi)^3} \frac{d\mathbf{p}_1'}{(2\pi)^3} \frac{1}{2E_{\mathbf{p}_1} 2E_{\mathbf{p}_2} 2E_{\mathbf{p}_1'} 2E_{\mathbf{p}_2'}} \theta^<(\mathbf{p}_1)\theta^<(\mathbf{p}_2)\theta^>(\mathbf{p}_1')\theta^>(\mathbf{p}_2')$$
$$\times \delta(E_{\mathbf{p}_1} + E_{\mathbf{p}_2} + q_0 - E_{\mathbf{p}_1'} - E_{\mathbf{p}_2'})(\mathcal{T}^{\mu\nu}_d - \mathcal{T}^{\mu\nu}_e), \tag{4.7}$$

where we define $\mathcal{T}^{\mu\nu}_{d,e}$ by

$$\mathcal{T}^{\mu\nu}_{d,e} = \mathrm{Tr}_{(1,2)} \left[\bar{J}^\nu_{d,e} P_{d,e}(p_1', p_2') J^\mu_{d,d} P_{d,d}(p_1, p_2) \right] \tag{4.8}$$

with

$$P_d(a,b) = (\gamma \cdot \hat{a} + M)_{(1)} (\gamma \cdot \hat{b} + M)_{(2)},$$
$$P_e(a,b) = \frac{1}{(E_a + M)(E_b + M)} (\gamma \cdot \hat{a} + M)_{(1)} (\gamma \cdot \hat{b} + M)_{(2)} \tfrac{1}{8} (I_{(1,2)} + \sigma^{ij}_{(1)} \sigma_{ij(2)}) (I + \gamma^0)_{(1)} (I + \gamma^0)_{(2)}$$
$$\times (\gamma \cdot \hat{b} + M)_{(1)} (\gamma \cdot \hat{a} + M)_{(2)},$$
$$\bar{J}_{d,e} = \gamma^0_{(1)} \gamma^0_{(2)} J^\dagger_{d,e} \gamma^0_{(1)} \gamma^0_{(2)},$$
$$J_d(p_1, p_2, p_1', p_2') = J_e(p_1, p_2, p_2', p_1'),$$

and $I^{(1,2)}$ the identity operator in Dirac space for both particles 1 and 2. The isospin sum that is still present is carried out by means of traces in isospin space. To this end we write the full two-body current (3.20) as

$$J_d^\mu = F_{d_0}^\mu (i(\tau_{(1)} \times \tau_{(2)})^3) + F_{d_1}^\mu \mathcal{I}_1 + F_{d_2}^\mu \mathcal{I}_1^\dagger + F_{d_3}^\mu \mathcal{I}_2 + F_{d_4}^\mu \mathcal{I}_2^\dagger \tag{4.9}$$

with $\mathcal{I}_1 = \frac{2}{3}\tau_{(2)}^3 - i(\tau_{(1)} \times \tau_{(2)})^3$ and $\mathcal{I}_2 = \frac{2}{3}\tau_{(1)}^3 + i(\tau_{(1)} \times \tau_{(2)})^3$.

Interchange of the particle labels (1) and (2) gives

$$F_{d_0} \leftrightarrow -F_{d_0}, \quad F_{d_1} \leftrightarrow F_{d_3}, \quad F_{d_2} \leftrightarrow F_{d_4}.$$

If we use this symmetry we get for the direct term:

$$\sum_{\text{isospin}} \bar{J}_d^\nu J_d^\mu = 4\overline{F}_{d_0}^\nu F_{d_0}^\mu + \tfrac{8}{9}[\overline{F}_{d_1}^\nu F_{d_2}^\mu + \overline{F}_{d_2}^\nu F_{d_1}^\mu - (\overline{F}_{d_1}^\nu - \overline{F}_{d_2}^\nu)(F_{d_3}^\mu - F_{d_4}^\mu)] + \tfrac{8}{3}[\overline{F}_{d_1}^\nu F_{d_1}^\mu + \overline{F}_{d_2}^\nu F_{d_2}^\mu + (\overline{F}_{d_2}^\nu - \overline{F}_{d_1}^\nu)F_{d_0}^\mu$$
$$+\overline{F}_{d_0}^\nu (F_{d_2}^\mu - F_{d_1}^\mu)] + \{(1) \leftrightarrow (2)\}. \tag{4.10}$$

For the pionic contribution to the exchange term the isospin sum gives zero and we only have a pion-isobar interference term and an isobar term:

$$\sum_{\text{isospin}} \bar{J}_d^\nu J_e^\mu = \tfrac{8}{3}[(\overline{F}_{d_1}^\nu + \overline{F}_{d_2}^\nu)F_{e_0}^\mu + \overline{F}_{d_0}^\nu (F_{e_1}^\mu + F_{e_2}^\mu)] + \tfrac{8}{9}[3(\overline{F}_{d_1}^\nu F_{e_1}^\mu + \overline{F}_{d_2}^\nu F_{e_4}^\mu) + \overline{F}_{d_1}^\nu (F_{e_2}^\mu + F_{e_4}^\mu)$$
$$+\overline{F}_{d_2}^\nu (F_{e_1}^\mu + F_{e_3}^\mu) - (\overline{F}_{d_2}^\nu F_{e_2}^\mu + \overline{F}_{d_1}^\nu F_{e_3}^\mu)] + \{(1) \leftrightarrow (2)\}, \tag{4.11}$$

with $F_{e_i}(p_1, p_2, p_2', p_1') = F_{d_i}(p_1, p_2, p_1', p_2')$.

The form of Eqs. (4.10) and (4.11), with the explicit symmetry in the particle labels (1) and (2), allows us at a later stage, when we use the same symmetry in the final (numerical) integrals, to only evaluate the terms which appear explicitly in the expressions of Eqs. (4.10) and (4.11) and to multiply the final result with a factor two.

The evaluation of the traces in spinor space is very cumbersome. We made use of the algebraic computer program FORM [17] to evaluate the traces in the object $r_{1_\mu} r_{2_\nu} \mathcal{T}^{\mu\nu} \equiv \mathcal{T}$ (r_1 and r_2 denote two dummy four vectors). In this program built-in rules for the evaluation of traces of products of γ matrices are available. Furthermore it is very suited for those cases where the number of terms in intermediate stages of the calculation is very large, as is the case here. The result is typically a polynomial of scalars that can be constructed from the (not necessarily independent) set of four-vectors.

The transverse amplitude squared $\mathcal{R}_T$ is obtained if we identify in $\mathcal{T}$:

$$r_1 \cdot r_2 = -2,$$
$$r_1 \cdot v_1 \, r_2 \cdot v_2 = \mathbf{v}_1 \cdot \mathbf{v}_2 - \frac{\mathbf{v}_1 \cdot \mathbf{q} \, \mathbf{v}_2 \cdot \mathbf{q}}{\mathbf{q}^2}$$

and the longitudinal $\mathcal{R}_L$ if we use

$$r_1 \cdot r_2 = 1,$$
$$r_1 \cdot v_1 \, r_2 \cdot v_2 = v_{1_0} v_{2_0}$$

for two arbitrary four-vectors v_1 and v_2. From the above expressions we already see that terms in $W^{\mu\nu}$ proportional to q^μ do not contribute to the transverse response, which simplifies the calculations considerably.

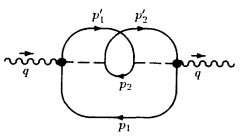

FIG. 7. Feynman diagram representing the exchange contribution corresponding to diagram (a) of Fig. 5.

Depending on the specific diagram under consideration, the number of terms in the final results can range from about one hundred to tens of thousands. Because of these large numbers, it is useless to present them in their explicit form. This raises the question how we can convince both the reader and ourselves that the results are correct. The most important way to do this is to compare with the static limit (SL) results which, much to our benefit, are extensively discussed by Van Orden and Donnelly [8]. For the algebraic part of the computer work this amounts to verifying that the SL of the full response functions coincides with the one they present. This comparison can be found in the next section.

The final step in the calculation of $W_{\text{2p2h}}^{\mu\nu}$ is the evaluation of the momentum integrals appearing in Eq. (4.7). This nine-dimensional integral can be reduced to seven dimensions if we use the energy conserving delta function and the fact that, if one uses spherical coordinates, one can transform the three azimuthal angles, with respect to $\mathbf{q}$, such that the integrand only depends on two of them, allowing a trivial integration of the third. The resulting seven-dimensional integral is handled with Monte Carlo techniques. This allows for a very straightforward treatment of the remaining step function $\theta^>(\mathbf{p}_2')$, which in other integration schemes gives rise to a complicated boundary structure. Again the question arises how we can gain confidence in the obtained result and it is once more the static limit that provides us with the strongest test on the numerical integration. Since the SL result [Eq. (5.11), to be derived in the next section] only depends on the relative momenta, a further reduction of the number of integration dimensions to two is possible. This procedure is quite cumbersome, but is extensively discussed in [8]. This provides the possibility to calculate the SL result in two completely independent ways: first naive Monte Carlo integration in seven dimensions,

second by an algorithm suited for low-dimensional integrals (like Romberg integration) applied to the two-dimensional integral. Agreement within Monte Carlo uncertainties is obtained. The number of Monte Carlo (MC) points (and accordingly the amount of CPU time) necessary to obtain accurate results that allow for a comparison of this type is rather large: typically 10^6–10^7. To obtain accurate (1%) results for the full calculation, a number of MC points of the same order is necessary.

V. STATIC LIMIT

As mentioned in the Introduction, the static limit (SL) is a procedure that is applied to two-body currents to obtain a nonrelativistic result which is more easy to handle in practice. To obtain these nonrelativistic two-body currents we sandwich the expressions (3.3), (3.4), and (3.19) between positive-energy ingoing and outgoing Dirac spinors for particle one and two, and only keep the lowest-order term in a $|\mathbf{k}|/M$ expansion such that $k_0 = 0$. For the pionic MECs we have the replacements

$$\overline{U}(\mathbf{p}_i', s_i')(\not{k}_i\gamma^5)_{(i)}U(\mathbf{p}_i, s_i) \to \chi^\dagger_{s_i'}(-(\boldsymbol{\sigma}_{(i)}\cdot\mathbf{k}_i))\chi_{s_i}, \tag{5.1}$$

$$\overline{U}(\mathbf{p}_i', s_i')(\gamma^j\gamma^5)_{(i)}U(\mathbf{p}_i, s_i) \to \chi^\dagger_{s_i'}\sigma^j_{(i)}\chi_{s_i} \tag{5.2}$$

and

$$k_i^2 - m_\pi^2 \to -(\mathbf{k}_i^2 + m_\pi^2). \tag{5.3}$$

The static limit π MECs are then given by

$$\mathbf{J}_{\text{in-flight}} = i(\boldsymbol{\tau}_{(1)}\times\boldsymbol{\tau}_{(2)})^3\left(\frac{g_\pi}{2M}\right)^2 \times\frac{(\boldsymbol{\sigma}_{(1)}\cdot\mathbf{k}_1)(\boldsymbol{\sigma}_{(2)}\cdot\mathbf{k}_2)(\mathbf{k}_1-\mathbf{k}_2)}{(\mathbf{k}_1^2+m_\pi^2)(\mathbf{k}_2^2+m_\pi^2)} \tag{5.4}$$

$$\mathbf{J}_{\text{contact}} = i(\boldsymbol{\tau}_{(1)}\times\boldsymbol{\tau}_{(2)})^3\left(\frac{g_\pi}{2M}\right)^2 \times\left(\frac{(\boldsymbol{\sigma}_{(1)}\cdot\mathbf{k}_1)\boldsymbol{\sigma}_{(2)}}{\mathbf{k}_1^2+m_\pi^2} - \frac{(\boldsymbol{\sigma}_{(2)}\cdot\mathbf{k}_2)\boldsymbol{\sigma}_{(1)}}{\mathbf{k}_2^2+m_\pi^2}\right), \tag{5.5}$$

$$\mathbf{J}_\pi = \mathbf{J}_{\text{in-flight}} + \mathbf{J}_{\text{contact}}\,. \tag{5.6}$$

Before we proceed to determine the static limit of the isobar current, we discuss an ambiguity in the application of the SL to the spin projection operator appearing in the Δ propagator. A common and natural procedure, used for instance by Van Faassen [18], is to replace the numerator of the Δ propagator of Eq. (3.6) by the on-mass shell spin projection operator, and the denominator by the positive-energy part:

$$G^{\mu\nu}_\Delta(p) \simeq \frac{\hat{\not{p}} + M_\Delta}{2E^\Delta_{\mathbf{p}}(p_0 - E^\Delta_{\mathbf{p}})} \times\left(-g^{\mu\nu} + \frac{2}{3M_\Delta^2}\hat{p}^\mu\hat{p}^\nu - \frac{1}{3M_\Delta}(\hat{p}^\mu\gamma^\nu - \hat{p}^\nu\gamma^\mu) + \tfrac{1}{3}\gamma^\mu\gamma^\nu\right), \tag{5.7}$$

where the hat denotes the on-mass shell projection ($\hat{p}_0 = E^\Delta_{\mathbf{p}}$). If we take into account that the vertices with which this propagator is contracted obey the relation (3.9), we can effectively use

$$G^{\mu\nu}_{\Delta_{\text{eff}}}(p) \simeq \frac{\hat{\not{p}} + M_\Delta}{2E^\Delta_{\mathbf{p}}(p_0 - E^\Delta_{\mathbf{p}})}\left(-g^{\mu\nu} + \frac{2}{3M_\Delta^2}\hat{p}^\mu\hat{p}^\nu + \frac{1}{3M_\Delta}\hat{p}^\nu\gamma^\mu\right). \tag{5.8}$$

If one does this for the current given in Eq. (3.19), a nonrelativistic reduction of this current sandwiched between Dirac spinors gives

$$\mathbf{J}_\Delta = \frac{f_{\pi NN}f_{\pi N\Delta}f_{\gamma N\Delta}}{2Mm_\pi^2}\left[ib\left(\tfrac{2}{3}\tau_1^3(\mathbf{k}_1\times\mathbf{q})\frac{\boldsymbol{\sigma}_{(1)}\cdot\mathbf{k}_1}{\mathbf{k}_1^2+m_\pi^2} + (1\leftrightarrow 2)\right) - a\,\tfrac{1}{3}i(\boldsymbol{\tau}_{(1)}\times\boldsymbol{\tau}_{(2)})^3\left(\frac{\boldsymbol{\sigma}_{(1)}\cdot\mathbf{k}_1}{\mathbf{k}_1^2+m_\pi^2}(\mathbf{k}_1\times\boldsymbol{\sigma}_{(2)})\times\mathbf{q} - (1\leftrightarrow 2)\right)\right] \tag{5.9}$$

with

$$b = \frac{16}{3(M_\Delta - M)}, \qquad a = \frac{8}{3(M_\Delta - M)},$$

$$\mathbf{k}_1 = \mathbf{p}_1' - \mathbf{p}_1, \qquad \mathbf{k}_2 = \mathbf{p}_2' - \mathbf{p}_2.$$

Note that, in the static limit all energy dependence of the Δ propagator has disappeared. Furthermore, as was the case for the pion current, the SL isobar current only depends on the relative momenta $\mathbf{k}_1$ and $\mathbf{k}_2$. This result is not equal to the one derived by Van Orden and Donnelly [8]. The discrepancy can be phrased in terms of the constants a and b, which in their case would read: $b = 2(2M_\Delta + 3M)/(M_\Delta^2 - M^2)$ and $a = 2(2M_\Delta + M)/(M_\Delta^2 - M^2)$. This difference can be traced back to the treatment of the Δ propagator. Their result can be obtained if one approximates, in the SL procedure, the Rarita-Schwinger propagator (3.6) by

$$G^{\mu\nu}_\Delta(p) \simeq \frac{\not{p} + M_\Delta}{p^2 - M_\Delta^2}(-g^{\mu\nu}) \tag{5.10}$$

with $p_0 \simeq M$. In this approach one neglects terms of leading order when the term G^{00}_Δ is considered. Precisely these terms, in combination with the difference in the numerators of the propagator as a result of identifica-

tion $p_0 \simeq M$ versus $p_0 \simeq M_\Delta$, give rise to the above mentioned differences. Furthermore the SL current we derived above, Eq. (5.9), equals (apart from coupling constants) the isobar current derived by Hockert [19] some twenty years ago, which has subsequently been used many times in the literature.

Apart from this ambiguity, it is now straightforward to determine the static limit of the expression $\mathcal{T}$ defined previously. It should be emphasized that we apply the SL procedure at the level of $\mathcal{T}$, not at the level of the current operator. This ensures that a final comparison with the SL result for $\mathcal{T}$ as found by Van Orden and Donnelly, who applied the SL at the current level, really provides a strong test on our full results for $\mathcal{T}$. To cast our results in a form that can be compared with those of Van Orden and Donnelly, we frequently have to make use of the relation $\mathbf{q} = \mathbf{k}_1 + \mathbf{k}_2$. For the direct contribution to the transverse amplitude squared we thus find

$$\begin{aligned}\mathcal{R}_T = 64c_N^2 \Bigg[& 2\frac{\mathbf{k}_1^2}{(\mathbf{k}_1^2+m_\pi^2)^2} + \mathbf{k}_{1_T}^2 \left(2\frac{\mathbf{k}_1^2\mathbf{k}_2^2}{(\mathbf{k}_1^2+m_\pi^2)^2(\mathbf{k}_2^2+m_\pi^2)^2} - 4\frac{\mathbf{k}_1^2}{(\mathbf{k}_1^2+m_\pi^2)^2(\mathbf{k}_2^2+m_\pi^2)} + \frac{1}{(\mathbf{k}_1^2+m_\pi^2)(\mathbf{k}_2^2+m_\pi^2)} \right) \Bigg] \\ & + 64c_\Delta^2 \mathbf{k}_1^2 \left(\mathbf{k}_1^2\mathbf{q}^2(2\tilde{b}^2+\tilde{a}^2) - (2\tilde{b}^2-\tilde{a}^2)(\mathbf{k}_1\cdot\mathbf{q})^2 \right) \frac{1}{(\mathbf{k}_1^2+m_\pi^2)^2} + 64c_\Delta^2 \tilde{a}^2 \frac{\mathbf{q}^4\mathbf{k}_{1_T}^2}{(\mathbf{k}_1^2+m_\pi^2)(\mathbf{k}_2^2+m_\pi^2)} \\ & + 64c_\Delta c_N \tilde{a} \left(\frac{4\mathbf{q}^2\mathbf{k}_1^2\mathbf{k}_{1_T}^2}{(\mathbf{k}_1^2+m_\pi^2)^2(\mathbf{k}_2^2+m_\pi^2)} - 2\frac{\mathbf{q}^2\mathbf{k}_{1_T}^2}{(\mathbf{k}_1^2+m_\pi^2)(\mathbf{k}_2^2+m_\pi^2)} - 4\frac{\mathbf{k}_1^2\mathbf{k}_1\cdot\mathbf{q}}{(\mathbf{k}_1^2+m_\pi^2)^2} \right) + (1 \leftrightarrow 2) \end{aligned} \tag{5.11}$$

with $c_N = (f_{\pi NN}/m_\pi)^2$, $c_\Delta = f_{\pi NN}f_{\pi N\Delta}f_{\gamma N\Delta}/(2Mm_\pi^2)$ (understood to be multiplied with the relevant form factors), $\mathbf{k}_{1_T}^2 = \mathbf{k}_1^2 - (\mathbf{k}_1\cdot\mathbf{q})/(\mathbf{q}^2)$ and $\tilde{a} = 2a/3$, $\tilde{b} = 2b/3$. Note that one has $\mathbf{k}_{2_T}^2 = \mathbf{k}_{1_T}^2$. This form allows for a direct comparison with the result of Van Orden and Donnelly, thus providing a severe test on our full result.

VI. RESULTS AND DISCUSSION

It is the aim of this section to compare calculations with calculations: we want to compare the results of the calculations of the full two-body current with those of the SL current, without yet confronting them with experimental data. We postpone this till Sec. VII, when we also have, apart from the quasifree knockout and the two-body contribution, the evaluation of a third important reaction channel at our disposal: production of a real (physical) pion in the final state. We think that the above mentioned comparison is interesting in itself, since it shows the importance of our relativistic treatment compared with the SL, as well as the basic systematics of the calculations.

In Fig. 8 the solid line shows the result of the full calculation of the 2p2h contribution to the transverse response function, the dotted line is the SL result. In these calculations, the three-momentum transfer is fixed at $|\mathbf{q}| = 550$ MeV/c and $|\mathbf{q}| = 1140$ MeV/c, respectively. At this moment, we leave out the Pauli exchange contribution. Since these two kinematics will return at several places, we will refer to them as kinematics I and II, respectively. There are two parameters to be specified: first the Fermi momentum in these calculations (and all to come) is given by 1.3 fm^{-1}, the binding energy per particle-hole pair is taken to be 35 MeV. This will become of relevance later when we compare with data. Furthermore these results are obtained for mass number $A = 56$ (the results, at fixed Fermi momentum, trivially scale with A).

Figure 8 clearly displays the large differences that occur in the two calculations. The sizable increase of the response at large energy transfer in the full calculation with respect to the SL calculation originates almost completely from the difference in the treatment of the propagator of the Δ isobar. Since, in our calculations, its full energy and momentum dependence is maintained, it is possible for the isobar current to show a resonance behavior: p^2 can become equal to M_Δ^2, whereas in the SL calculation $p^2 = M^2$. The latter choice clearly discards all dependence on the dynamics of the Δ-isobar propagator. It is this feature that gives the large enhancement of the full result with respect to the SL and which is missing in the original work of Van Orden and Donnelly [8]. To display this effect more clearly, we also show in Fig. 9 what happens if we try to account for this resonating behavior by hand in the SL calculation. To this end we modify the scalar (denominator) part of the Δ propagator in the SL current such that it equals the one of the

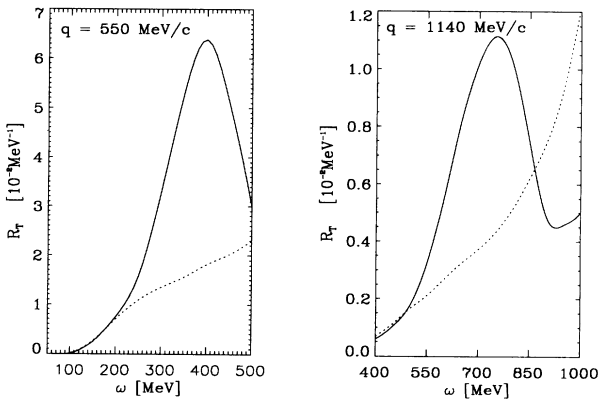

FIG. 8. Comparison of the contribution of the full two-body current to the transverse response (solid line) with that of the static-limit current (dotted line). The momentum transfer is 550 MeV/c (left figure) and 1140 MeV/c (right figure). The atomic mass number is 56, the Fermi momentum 1.3 fm^{-1}. The Pauli exchange contribution is not included.

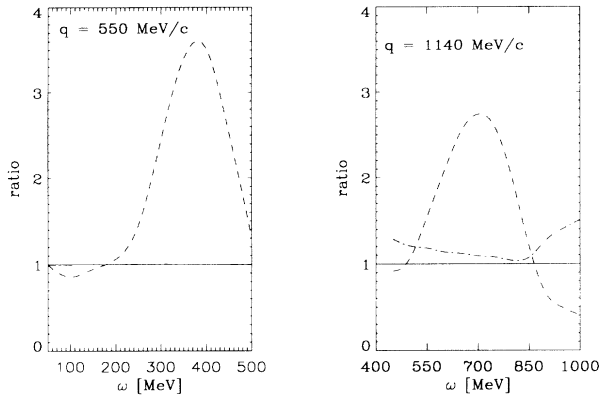

FIG. 9. Ratio of the full two-body calculation results to the SL results for the transverse response function at a momentum transfer of $|\mathbf{q}| = 550$ MeV/c and $|\mathbf{q}| = 1140$ MeV/c, respectively (dashed lines). The dash-dotted lines represent the ratio of the full to the resonating static limit (RSL) (see text). The solid lines (unity) are plotted as reference. The Pauli exchange contribution is not included.

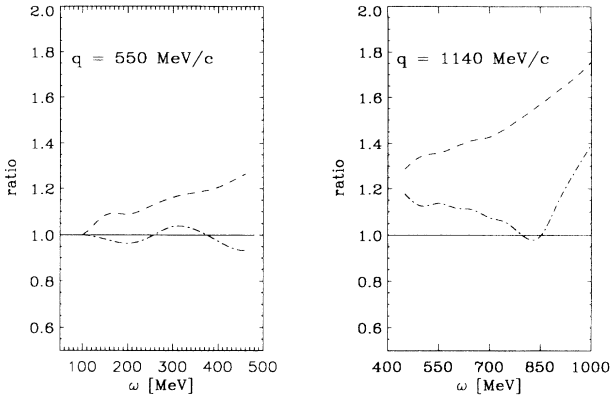

FIG. 10. Ratio of the full pion MEC calculation results to the SL results for the transverse response function at a momentum transfer of $|\mathbf{q}| = 550$ MeV/c and $|\mathbf{q}| = 1140$ MeV/c, respectively (dashed lines). The dash-dotted lines represent the ratio of the full Δ-isobar current contribution to the resonating static limit (RSL) of the Δ isobar (see text), the solid lines (unity) are plotted as reference.

full calculation, but we keep the rest of the SL current as it is:

$$\frac{1}{2M_\Delta(M - M_\Delta)} \rightarrow \frac{1}{p^2 - M_\Delta^2 + iM_\Delta\Gamma(s = p^2)}$$

with $p^2 = (p_1 + q)^2 = M^2 + q^2 + 2p_1 \cdot q$. We refer to a calculation of this type as the resonating static limit (RSL). Note that a calculation of the RSL does not allow anymore for a reduction of the number of integration dimensions to two; the calculation has to be performed in seven dimensions. In Fig. 9 the dash-dotted line represents the ratio of the full calculation to this RSL, for both kinematics I and II. For kinematics I the resulting ratio is almost unity and the differences can hardly be seen at the scale of the plot. For kinematics II there are clearly still differences between the RSL and full calculation at the 20% scale. This is to be expected since here the higher-order terms in an expansion in $|\mathbf{q}|/M$ will be more important. At this stage one can think of an even simpler prescription to extend the SL calculation to account for the resonating behavior: neglect of the initial nucleon momentum $\mathbf{p}_1$. This would amount to a replacement as the one given above, but with $p^2 = M^2 + q^2 + 2M\omega$. Since in that case the integrand still only depends on $\mathbf{k}_1$ and $\mathbf{k}_2$, the reduction procedure to two dimensions remains applicable, which would make it a very useful approximation. It does not work in practice, however. The resonance structure for kinematics I one obtains that way has a considerably smaller width and larger maximum than the results of the RSL and full calculations. We therefore conclude that this tentative way to approximate the resonance behavior is unreliable.

In Fig. 10 we show the effect on the pion and isobar currents separately for the two kinematics. For the pionic current we see that the full result is generally larger than the SL, and that the relative difference increases with momentum transfer. For the isobar current alone, the relative effects also increase with momentum transfer, although their behavior is more complex.

The evaluation of the exchange contribution was restricted to the term which shows the resonance behavior. We refer to this term as the s-channel Pauli exchange contribution. In Fig. 11 we show the importance of this Pauli exchange contribution to the response function. The solid curve denotes the full result, whereas the dotted curve shows the direct term only. The difference is thus due to the exchange contribution. The dash-dotted and the dashed line show the same for the SL. In the SL the exchange term is almost negligible. Since the exchange term shows the resonance behavior, its contribution in the full calculation, however, is pretty large and, when it comes to quantitative results, cannot be discarded.

One could raise the question whether it is sufficient to consider only the pion contribution to the meson exchange currents. It is well known that the ρ meson, despite its much larger mass, can play an important role

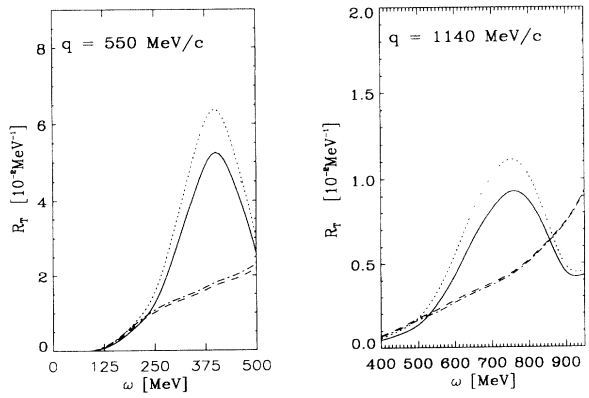

FIG. 11. Effect of the s-channel Pauli exchange term on the transverse response functions for both kinematics I and II. The SL result is hardly affected, the full results decrease considerably.

in calculations that deal with meson exchange current effects on nuclear properties. This is due to the large anomalous coupling term ($q_\mu \sigma^{\mu\nu}$) of the ρ-meson vector-field to the nucleon field. To get an idea of its importance in the two-body knockout channel, we calculated the ρ current contribution to $W^{\mu\nu}$ (thus ignoring the interference terms with the two-body currents we discussed until now). With the formalism of this section it is straightforward to evaluate this contribution, again without the necessity to apply the static limit. To determine the ρ MEC we used minimal substitution in the usual ρNN Lagrangian. At this point there are other model treatments which can give differences in the resulting currents up to a factor two [20]. For kinematics I, the resulting ρ MEC (two-particle knockout) contribution to the transverse response ranges from one-tenth at $\omega = 200$ MeV to one-third at $\omega = 500$ MeV of the π MEC contribution. For kinematics II, it ranges from one-fifth at $\omega = 500$ MeV to one-half at $\omega = 1000$ MeV of the π MEC contribution. Since the π MEC itself gives only a small contribution compared to the other reaction channels (for instance, its contribution to R_T is 0.23×10^{-2} MeV^{-1} at $\omega = 200$ MeV in the full calculation), we can safely ignore the ρ contribution in the rest of this work.

Finally a few words on the systematics of the calculations. We already noted that generally the relativistic effects increase with momentum transfer. Furthermore, if one decreases the Fermi momentum to 1.2 fm^{-1}, the results of the full calculation tend to decrease considerably. The calculations are quite sensitive to the specific values of the cutoffs appearing in the form factors. We would like to stress however that, as is discussed in Appendix A, we determined all of these from independent sources and did not treat them as free parameters.

VII. REAL-PION PRODUCTION

Since, for large energy transfer, the production of an on-shell (real) pion becomes possible, the latter process should also be considered before a meaningful comparison with experimental data can be made. In this section we describe the way we treat this important channel in our calculations.

A. Effective Lagrangian vs isobar-model approaches

There exists a number of different ways to describe real-pion electroproduction. From πN scattering it is a very well established fact that the πN system has a strong resonance in the spin- and isospin-$\frac{3}{2}$ channel of p-wave character, which is the Δ resonance that we discussed in much detail in the previous sections. The quantum numbers of the photon allow for the excitation of this nucleon resonance and this appears to be the dominant mechanism for pion photoproduction and electroproduction [21,22]. It is the spirit of isobar models to use this feature for a description of the nucleon and nuclear response in the pion production region via the excitation and propagation of a Δ isobar, which is treated as a separate degree of freedom. The Δ isobar cannot exist as an asymptotic state, however. It mainly decays into a πN final state. In the isobar model this decay is implicitly accounted for by the inclusion of a complex part in the propagator (the width). In the case of nuclei the propagation of the Δ isobar can be further modified to include the effects of the interaction between the Δ isobar and the nuclear environment. This is the main content of the Δ hole model [23] which has been applied with success in pion electroproduction and photoproduction as well as pion absorption, which shows once more the underlying idea that all these different scatterers essentially probe the Δ resonance. In a forthcoming paper [24] we will discuss the Δ hole model and its connection with the approach of the previous sections in more detail.

A second approach is based on effective Lagrangians [8]. There are two main differences between this approach and the isobar model. First the decay of the Δ isobar is explicitly accounted for, i.e., the pion and the nucleon degree of freedom in the final state are treated as the final state of the scattering process. In an inclusive calculation this means that one has to sum explicitly over all possible final states which exist of a real pion and a nucleon. This leads to the second important difference: there are more processes than Δ isobar excitation alone that can contribute to real-pion production. For instance, there are (nucleon) Born terms present that are extremely important to obtain correct results at threshold, both from an experimental (comparison with data) and a theoretical point of view (comparison with low-energy theorems). In the resonance region, however, pion production via an intermediate Δ isobar is the dominant process, although the nonresonant Born terms give a background contribution that is nonnegligible. In summary: contrary to the isobar model, the πN final state is treated explicitly in the effective Lagrangian approach.

We choose to follow the effective Lagrangian approach. Since we are not interested in threshold effects, we only consider the two diagrams of Fig. 12 where in both cases an intermediate Δ isobar is formed. The second, crossed diagram does not give a resonant contribution and already accounts for a considerable part of the background. Because of our choice to neglect the Born diagrams, direct comparisons with isobar models can and will be made at several places.

B. Contribution of the real-pion production current to $W^{\mu\nu}$

It is now straightforward to write down the current for real-pion production for the diagrams of Fig. 12. With the aid of the rules given in the previous section we obtain:

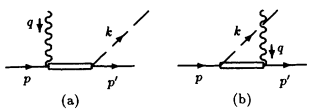

FIG. 12. Feynman diagrams for the real-pion production process via an intermediate Δ-isobar excitation.

$$J^{\mu\,a}_{\pi\text{prod}} = c_\pi \Big(\mathcal{I}^a k_\alpha \mathcal{F}^{\alpha\beta} G_{\Delta_{\beta\delta}}(p+q) \mathcal{G}^{\delta\mu} - (\mathcal{I}^\dagger)^a \mathcal{G}^{\mu\delta} G_{\Delta_{\delta\beta}}(p'-q) \mathcal{F}^{\beta\alpha} k_\alpha \Big) = c_\pi \Big(\mathcal{I}^a F^\mu_{\text{dir}} - (\mathcal{I}^\dagger)^a F^\mu_{\text{cross}} \Big) \qquad (7.1)$$

with

$$\mathcal{I}^a = T^a (T^\dagger)^3 = \tfrac{2}{3}\tau^a - \tfrac{1}{3} i \epsilon_{a3b} \tau^b$$

and

$$c_\pi = \frac{f_{\gamma N\Delta} f_{\pi N\Delta}}{2 M m_\pi} F_{\gamma N\Delta}(q^2) R(r^2).$$

The label a is the isospin label of the produced pion. The momenta are defined in the diagrams, the form factors in Appendix A. Applying the formalism of Sec. IV, we find for the contribution of this current to $W^{\mu\nu}$

$$W^{\mu\nu}_{\pi\text{prod}} = V \int \frac{d\mathbf{p} d\mathbf{k}}{(2\pi)^6 2 E^\pi_{\mathbf{k}}} \frac{M^2}{E_{\mathbf{p}_1} E_{\mathbf{p}_1'}} \delta(\omega + E_{\mathbf{p}_1} - E^\pi_{\mathbf{k}} - E_{\mathbf{p}_1'}) \theta^<(\mathbf{p}_1) \theta^>(\mathbf{p}_1') \mathcal{O}^{\mu\nu}_{\pi\text{prod}} \qquad (7.2)$$

with

$$\mathcal{O}^{\mu\nu}_{\pi\text{prod}} = c_\pi^2 \tfrac{4}{3} \Big(\text{Tr}[\bar{F}^\nu_{\text{dir}} \Lambda^+(\mathbf{p}_1') F^\mu_{\text{dir}} \Lambda^+(\mathbf{p}_1) + \bar{F}^\nu_{\text{cross}} \Lambda^+(\mathbf{p}_1') F^\mu_{\text{cross}} \Lambda^+(\mathbf{p}_1)] - \text{Tr}[\bar{F}^\nu_{\text{cross}} \Lambda^+(\mathbf{p}_1') F^\mu_{\text{dir}} \Lambda^+(\mathbf{p}_1) + \bar{F}^\nu_{\text{dir}} \Lambda^+(\mathbf{p}_1') F^\mu_{\text{cross}} \Lambda^+(\mathbf{p}_1)] \Big) . \qquad (7.3)$$

As in the previous section, the traces are evaluated with the aid of FORM and confidence in the results was gained through comparisons of parts of the results with [8,12]. The six-dimensional integral in Eq. (7.2) can be reduced to a four-dimensional one which subsequently is evaluated with Monte Carlo integration. Convergence is obtained with a number of integration points of the order of 10^4. Confidence in the numerical results was gained by a comparison with the analysis of Van Orden and Donnelly. In their analysis they neglect the three-momentum of the initial nucleon in the expression of $\mathcal{O}^{\mu\nu}$. This enables one to integrate analytically over $\mathbf{p}$ and to reduce the number of integration dimensions to two. This integration, which for the angular part of the integral is rather cumbersome, is, again much to our benefit, discussed in detail in [8]. We will refer to the amplitude obtained this way as the reduced amplitude. In Fig. 13 we compare this calculation (dashed), which involves a Romberg integration in two dimensions, with a Monte Carlo integration in four dimensions where the same approximation with respect to the initial nucleon momentum is made (dotted). In this figure the solid curve is the Monte Carlo result *without* the latter approximation. As one can see from the figure, the effect of this simple, but, to obtain the reduced amplitude, essential approximation is a reduction of the cross section in the resonance region of about 20%. The two results are not completely identical since there remains a subtle difference in the approximations that are made with respect to the initial nucleon momentum $\mathbf{p}$: it is not possible to treat the Fermi gas phase-space equally in both treatments.

The calculations that are displayed in Fig. 13 were all performed with a fixed Δ-isobar decay width of 120 MeV. The results change considerably if these calculations are done with an energy-dependent width. In general the cross section increases more rapidly at the low-ω side of the peak at the expense of producing a smaller cross section at the high-ω side of the peak. (This might seem counterintuitive, but one must remember that, in the present approach, the parametrization of the width only influences the denominator of the Δ-isobar propagator. The energy-dependent width is smaller than the fixed width below the resonance peak, but larger above the resonance peak. Thus the above effect can be understood. For a consistent calculation, however, changes in the decay width should also be reflected in the $\pi N\Delta$ vertex which appears in the matrix element.) In the next

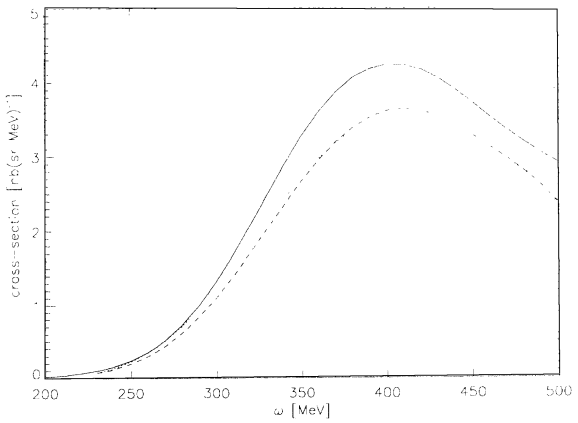

FIG. 13. Comparison of real-pion production cross sections calculated with four-dimensional Monte Carlo integration (dashed curve) with a calculation of the two-dimensional integration of the reduced amplitude (see text, dotted), where in both cases the initial nucleon momentum is neglected. The solid line denotes the Monte Carlo integration results without the latter approximation.

section we discuss the meaning and the importance of the energy dependence of the Δ-isobar decay width in more detail.

C. Comparison with the isobar model

As mentioned above, there exists an alternative way to describe pion electroproduction: the isobar model, or, extended to complex nuclei, the Δ-hole model. The main difference with respect to our treatment is that one does not treat the πN final state explicitly; the amplitude squared that appears in the calculation of the response tensor is simply the square of the $\gamma N \to \Delta$ transition vertex. The decay into the πN final state is then implicitly accounted for either by the inclusion of an imaginary part (the decay width) in the Δ-isobar propagator [23] or by the convolution with a Breit-Wigner resonance shape [25]. In this section we want to discuss the connection between the latter treatment and ours.

1. *Relation between isobar model and effective Lagrangian approach*

The key ingredient of this discussion is the following relation, which can be obtained from Dyson's equation with self-energy Σ for G_Δ and the complex conjugate Dyson's equation (suppressing Dirac indices):

$$\mathrm{Im}(G_\Delta) = \overline{G}_\Delta \mathrm{Im}(\Sigma) G_\Delta, \tag{7.4}$$

where the bar denotes the Dirac adjoint of G_Δ. If we apply this to the case under consideration, a shorthand notation for the isobar model would be

$$W^{\mu\nu} = \frac{V}{\pi} \mathrm{Im}\left(\overline{\Gamma}^\nu G_\Delta \Gamma^\mu\right), \tag{7.5}$$

whereas a shorthand notation for our effective Lagrangian model would read

$$W^{\mu\nu} = \frac{V}{\pi} \overline{\Gamma}^\nu \overline{G}_\Delta \mathrm{Im}(\Sigma_{\pi N}) G_\Delta \Gamma^\mu. \tag{7.6}$$

Here Γ^μ denotes the $\gamma N \to \Delta$ transition vertex. We see that according to Eq. (7.4) both treatments should give identical results *provided* the imaginary part of the Δ-isobar propagator in the isobar model is generated dynamically via Dyson's equation.

We now work out this statement in more detail. We start with the left-hand side (LHS) of Eq. (7.4), which we write as (suppressing isospin)

$$\mathrm{LHS} = \mathrm{Im}\left[-i\left(\frac{f_{\gamma N\Delta}}{m_\pi}\right)^2 \int \frac{d^4p}{(2\pi)^4} \mathrm{Tr}[\mathcal{G}^{\nu\alpha} G_{\Delta_{\alpha\beta}}(p) \mathcal{G}^{\beta\mu} \times G_D(p-q)]\right] \tag{7.7}$$

with G_D the density-dependent part of the Fermi gas propagator [cf. Eq. (2.6)], $\mathcal{G}^{\beta\mu}$ the $\gamma N\Delta$-vertex and $G_{\Delta_{\alpha\beta}}(p)$ the isobar propagator which we write as

$$G_{\Delta_{\alpha\beta}}(p) \equiv \frac{p^2 - M_\Delta^2 + i\Gamma(s) M_\Delta}{(p^2 - M_\Delta^2)^2 + [\Gamma(s) M_\Delta]^2} \Pi_{\Delta_{\alpha\beta}}(p).$$

Here we include the energy-dependent width as derived in Sec. III B. Note that at this point an approximation has been made, since, when we derived the energy-dependent width, we averaged over spin. Multiplying with $\int ds \delta(s - p^2)$ we can write Eq. (7.7) as

$$\mathrm{LHS} = \int \frac{ds}{\pi} \frac{\Gamma(s) M_\Delta}{(p^2 - M_\Delta^2)^2 + [\Gamma(s) M_\Delta]^2} \frac{d\mathbf{p}}{(2\pi)^3 2\tilde{p}_0} \times \mathrm{Tr}\left[\mathcal{G}^{\nu\alpha} \Pi_{\Delta_{\alpha\beta}}(\tilde{p}) \mathcal{G}^{\beta\mu} \frac{-iG_D(\tilde{p}-q)}{2\pi}\right] \tag{7.8}$$

with $\tilde{p}_0 = \sqrt{s + \mathbf{p}^2}$. Equation (7.8) is indeed the convolution of the $\gamma N \to \tilde{\Delta}$ matrix element squared, where $\tilde{\Delta}$ denotes a Δ isobar with invariant mass $W \equiv \sqrt{s}$, with a Breit-Wigner resonance shape. The latter contains the energy-dependent width obtained from the imaginary part of the self-energy $\Sigma_{\pi N}$. The latter should include a correction due to Pauli blocking of the nucleon in the final state.

If we multiply Eq. (7.8) with $\frac{V}{\pi}$ we obtain the expression for $W^{\mu\nu}_{\pi\mathrm{prod.}}$ in the isobar model [25]. (As has been remarked when we derived the Δ isobar decay width, the isospin factor in this case equals 1.)

The right-hand side (RHS) of Eq. (7.4) can be written as

$$\mathrm{RHS} = c_\pi^2 \int \frac{d^4p}{(2\pi)^4} \mathrm{Tr}[\mathcal{G}^{\nu\alpha} G_{\Delta_{\alpha\beta}} \mathrm{Im}\left(\int \frac{d^4k}{(2\pi)^4} k_\delta \mathcal{F}^{\delta\beta} G_P(p-k) \mathcal{F}^{\epsilon\gamma} k_\gamma\right) G_{\Delta_{\epsilon\chi}} \mathcal{G}^{\chi\mu} G_H(p-q)]. \tag{7.9}$$

If we focus on the pole structure, performing the contour integrations over p_0 and k_0, we obtain

$$\mathrm{RHS} = c_\pi^2 \pi \int \frac{d\mathbf{p}d\mathbf{k}}{(2\pi)^6 2E_{\mathbf{k}}^\pi} \frac{M^2}{E_{\mathbf{p}-\mathbf{q}} E_{\mathbf{p}-\mathbf{k}}} \theta^<(\mathbf{p}-\mathbf{q}) \theta^>(\mathbf{p}-\mathbf{k}) \mathrm{Tr}[\mathcal{G}^{\nu\alpha} G_{\Delta_{\alpha\beta}} k_\delta \mathcal{F}^{\delta\beta} \Lambda^+(\mathbf{p}-\mathbf{k}) \mathcal{F}^{\epsilon\gamma} k_\gamma G_{\Delta_{\epsilon\chi}} \mathcal{G}^{\chi\mu} \Lambda^+(\mathbf{p}-\mathbf{q})]. \tag{7.10}$$

If we shift the integration variable $\mathbf{p}$ to $\mathbf{p}+\mathbf{q}$, multiply with $\frac{V}{\pi}$ and include the isospin factor $\frac{4}{3}$ [cf. Eq. (7.3)], we obtain the same expression as the direct contribution in Eq. (7.2). We may now conclude that a convolution in the isobar model with an energy-dependent width $\Gamma(s)$ must give the same result as a calculation where one explicitly sums over all possible final pion states via direct Δ-isobar production. In other words, the energy dependence of the width effectively accounts for the phase space that is available to the produced pion. This then raises the question why one would do a calculation of our type, since it is technically much more involved than the isobar model calculation. An advantage of the effective Lagrangian approach is that it is clear from the outset how to incorporate other production mechanisms (like the Born diagrams) and the interferences with the direct Δ-isobar contribution [interference term of diagrams (a) and (b) in Fig. 12] are consistently taken into account. At threshold these effects are presumably very important. Although we do not include the Born terms, the argument in favor of the effective Lagrangian approach already applies in our case, since we include besides the Δ-isobar direct term, also the Δ-isobar crossed term and their interference term. Still, the present analysis is a strong argument to refrain from a complicated effective Lagrangian calculation, especially in the resonance region and to apply the isobar model, *provided one uses the energy-dependent width.*

2. Numerical results

For the $\gamma N\Delta$ coupling of Jones and Scadron [15] that has been used by Wehrberger, Bedau, and Beck [26] we will explicitly (numerically) check the statements we made above. There are a few reasons to do this. First, we believe that a demonstration of the equivalence of the two approaches described above is useful and illuminates many statements in the literature that are often taken for granted when it comes to the treatment of the resonant nature of the Δ isobar. Second, this analysis will give better insight into the importance of form factors at high momentum transfer, especially the form factor $R(r^2)$ that depends on the relative πN momentum (for a more detailed discussion of this form factor see Appendix A).

In the present analysis we use the different $\gamma N\Delta$ coupling of [15] with respect to the previous section, in order to facilitate comparison with the study in [25]. It is given by

$$\tilde{\mathcal{G}}^{\beta\mu}=\tilde{c}\Big[M_\Delta(-q^\beta\gamma^\mu+\not{q}g^{\beta\mu})+q^\beta k^\mu-q\cdot kg^{\beta\mu}\Big]\gamma^5. \tag{7.11}$$

The differences are that the constraint of Eq. (3.9) is not incorporated and the second term, proportional to the Δ-isobar momentum k, is absent in Peccei's coupling. The coupling constant in this analysis is given by

$$\tilde{c}=\frac{1}{M(M_\Delta+M)}\sqrt{\tfrac{3}{2}}3.0G(q^2) \tag{7.12}$$

with

$$G(q^2)=\left(\frac{1}{1-\frac{q^2}{(M_\Delta+M)^2}}\right)\left(\frac{1}{1-\frac{q^2}{0.71\ \mathrm{GeV}^2}}\right)^2\times\left(\frac{1}{1-\frac{q^2}{3.5\ \mathrm{GeV}^2}}\right)^{\frac{1}{2}}.$$

If the difference in isospin conventions is taken into account, this coupling is almost equal to the value of Peccei: their ratio is given by 1.02. When these changes are accounted for, all previous formulas still apply, and a numerical evaluation is now straightforward to carry out. The trace algebra is again carried out with FORM, the numerical integrations with Monte Carlo methods. To simplify the comparison we ignored the Pauli blocking in both the isobar and effective Lagrangian approach.

In Fig. 14 we compare the results of the effective Lagrangian approach (dotted line) with the convolution approach of Wehrberger and Beck (solid line) for kinematics I and II. The two curves are in both cases almost indistinguishable. To achieve this, it is of vital importance to have an energy-dependent width in the convolution approach that is consistent with the $\pi N\Delta$ vertex used in the effective Lagrangian calculation.

By virtue of the present comparison, some extra information was gained in the case of kinematics II. If a calculation in the effective Lagrangian approach is carried out without the form factor $R(r^2)$ (see Appendix A), but with a reasonable parametrization of the width like the Bransden-Moorhause parametrization, the resulting response at high energy transfer ω is a factor four larger than in the present treatment. This shows two things. First, as emphasized earlier, a consistent treatment of the $\pi N\Delta$ coupling and the decay width is essential in an effective Lagrangian approach. Second, the form factor $R(r^2)$ is necessary to obtain reasonable results for the real-pion production part of the response-functions in the 1 GeV region of kinematics II.

At this stage we finally want to point out that the

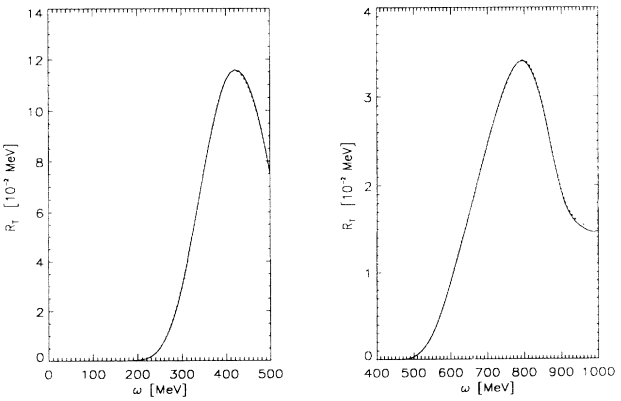

FIG. 14. Comparison of the effective Lagrangian approach (dotted line, where the pion in the final state is explicitly accounted for) with the convolution approach (solid line, where the decay is treated implicitly through incorporation of the energy-dependent width) of Wehrberger and Beck.

discussion above has considerable consequences for the results obtained by Rost, Price and Shepard in [27]. For a detailed discussion of this issue, however, we refer to our forthcoming paper [24] or to [28].

VIII. COMBINED MODEL RESULTS

A. The combined results

Here we present the combined response of the reaction channels that we described extensively in the previous sections and make a first comparison with experimental data. We start with a short survey of the three channels involved.

Quasifree knockout of a single nucleon, due to the one-body nucleon current (to be represented by dash-dotted lines). The (elementary) derivation of this contribution will not be given in this paper (see, e.g., [28]). The results are identical to those of Moniz [29]. The nucleon form factors used are those of Gari and Krümpelmann [30].

Two-nucleon knockout due to the full two-body current, which includes the Pauli exchange contribution (to be represented by short-dashed lines). Two-nucleon knockout due to the static limit two-body current (to be represented by long-dashed lines).

Knockout of a single nucleon together with the production of an on-shell pion, through intermediate Δ-isobar production (to be represented by dash-triple-dotted lines).

As we explained in Sec. IV, at this level of approximation where no one-particle–one-hole excitations are accounted for in the nuclear ground state, we may add these contributions to $W^{\mu\nu}$ incoherently. Our results apply strictly taken only to infinite systems. We have one parameter that should be specified in this respect: the Fermi momentum. It is chosen such that the density (which is proportional to k_F^3) is in reasonable agreement with the average density of the nucleus under consideration. For ^{12}C a typical value is 1.1 fm^{-1}, for ^{56}Fe 1.3 fm^{-1}, and for ^{208}Pb 1.35 fm^{-1}.

In Fig. 15 we compare the combined response of these three channels (the solid line) with the data for the transverse response function of ^{56}Fe for kinematics I ($|\mathbf{q}| = 550$ MeV). The most striking result is the large contribution of the full two-body current in and beyond the dip region. This is, as we explained and discussed in the previous section, completely due to the resonating isobar contribution. It is this effect that brings us a long way in explaining the experimentally observed strength in the dip region [2]. For comparison we show the result one would obtain for the total response when, instead of the full two-body current contribution, the SL result would be used (dotted line). Apart from some minor details this is what one obtains in the original analysis of Van Orden. Clearly the discrepancy with the data is larger. From these results we conclude that an important part of the strength of the transverse response function in the dip region is due to two-nucleon knockout via an intermediate Δ-isobar excitation.

To our knowledge there are two analyses in the literature where the authors claim that two-body currents do not or cannot play such an important role. In [27], on the basis of a rather phenomenological treatment of the Δ isobar, the authors conclude that one-body currents are sufficient to get agreement between theory and experiment in the dip region. As mentioned in Sec. VII C 2, we will discuss this claim in more detail in a forthcoming paper [24]. Here we note that the energy-*in*dependence of the Δ-isobar decay width in their analysis has rather large consequences for the conclusion drawn.

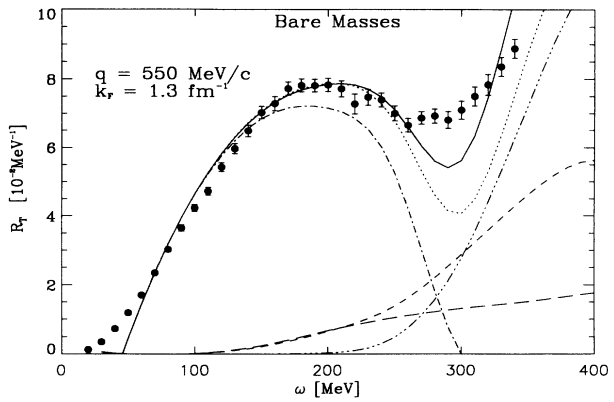

FIG. 15. Comparison of the combined transverse response (solid line) of the quasifree knockout (dash-dotted line), the pion production (dash-triple dotted line) and the full two-body knockout (dashed line) with the data of kinematics I for ^{56}Fe. Also displayed is the static-limit result for the two-body knockout contribution (long-dashed line). Finally, the dotted line shows the combined response one would obtain replacing the full two-body results with the SL two-body results. The data are taken from [5].

The second is described in two papers by Takaki [31], where he claims that two-body currents are not capable of accounting for the strength in the dip region [or for the case he considers, the $(e, e'p)$ reaction where one detects one knocked out proton, the excess strength at large missing energy]. His conclusion is that three-body processes (of unspecified origin) are to be held responsible for the missing strength. Takaki assumes that the matrix element of the scattering process is essentially constant, such that phase-space arguments apply. In the present analysis, however, we have seen that the latter assumption certainly does not hold for the isobar current as a consequence of the resonance behavior. We therefore believe that there is no contradiction between Takaki's conclusions and ours if this complication is taken into account.

In Fig. 16 we show similar results as in Fig. 15, but now at the much larger momentum transfer of kinematics II ($|\mathbf{q}| = 1140$ MeV). Although the comparison with the data is fair, it is not obvious that one needs the two-body current contribution that we calculate to obtain a reasonable description of the data. At the large energy transfer of more than 700 MeV, it is possible that the higher nucleon resonances that have a strong (transverse) electromagnetic coupling [$N(1520)$ and $N(1535)$] start to become important. The continuous rise of the data, combined with the disappearance of purely nucle-

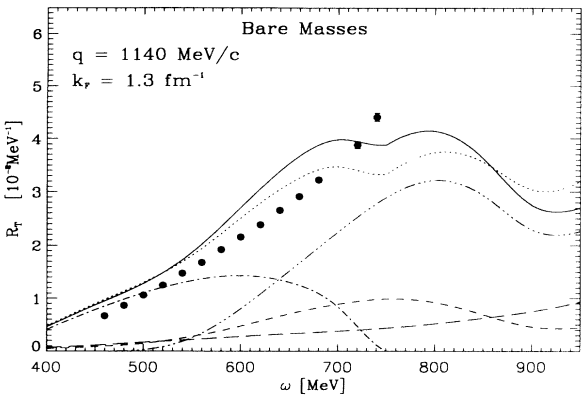

FIG. 16. Results as in Fig. 15, but now for kinematics II. The data are taken from [10].

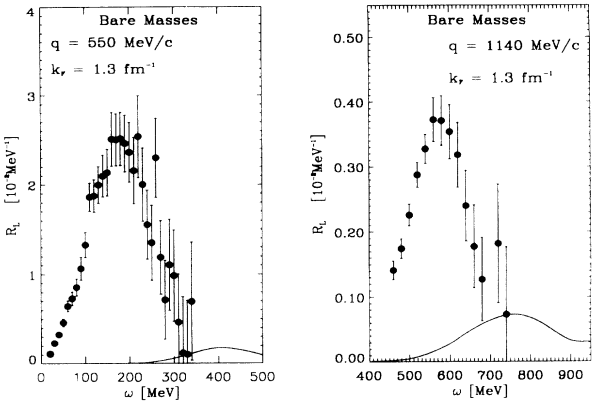

FIG. 17. Comparison of the contribution of the resonating part of the Δ-isobar two-body current (solid lines) to the longitudinal response, for kinematics I and II. These results are not meant to give an account of full-model results for R_L. Only one channel (two-body knockout) is displayed here (see text).

onic and Δ-isobar channels at least suggests that these other resonances will play a role.

As mentioned in the general introduction, the simultaneous description of the longitudinal and transverse response functions is one of the central goals one would like to achieve. The model we discuss at present will mainly affect the transverse response function. This is due to the fact that we study the physics of the nuclear current. Detailed studies of the longitudinal response functions in various models have shown that other physics there is important. For example, initial state correlations are found to be responsible for its quenching. It is beyond the scope of this paper to present "state of the art" results for the longitudinal response. In this respect, however, we have to consider the possibility that the large two-body contribution in R_T would also manifest itself in the longitudinal response. This could endanger the simultaneous understanding of the response functions, since, experimentally, the longitudinal response is very small at large energy transfer. Figure 17 is meant to show that indeed the contribution of the two-body isobar current to the longitudinal response remains small and stays, for both kinematics, well within the bounds set by the data. This figure is not meant, however, to present a full model description of the longitudinal response. From this we conclude that our predictions for the transverse response functions do not affect the longitudinal one in any severe way.

Finally, we present in Fig. 18 results of our calculations for a different type of data set: the transverse response (in mb) for fixed four-momentum $q^2 = 0.1$ GeV^2, which constitutes another slice in ω $|\mathbf{q}|$ space. Clearly the calculated response deviates considerably from the data at low energy transfer, but is very reasonable in the Δ-isobar resonance region. Without the full two-body contribution, the agreement would be much less. The discrepancy at low energy transfer can be understood once one examines the data for R_L (which we do not display, see [32]). These show a long tail into the high energy transfer region. Only beyond 300 MeV the data for R_L become compatible with zero This indicates that, presumably, one-body nucleon processes still play a role at ω values up to 300 MeV. On the other hand, in our simple Fermi gas calculations, the latter contribution vanishes already at $\omega = 200$ MeV. This clearly indicates one of the major shortcomings of the model as it is, and this observation leads us to the following.

B. Criticism

The present analysis would be incomplete without a thorough discussion of its main shortcomings. The most obvious one is the neglect of interactions of any type in both initial and final states. These lead, for the ground state, to particle-hole excitations, which give rise to high-momentum components in the nuclear wave function, or, equivalently, for an infinite system to depletion of the Fermi sea. These high-momentum components tend to enhance the tail of the response functions. The final-state interactions are found to change the response functions considerably [33]. In general they redistribute the strength such that the peak values are diminished and the tails of the quasifree knockout distributions broadened. Furthermore, in a mean-field sense, the interactions in

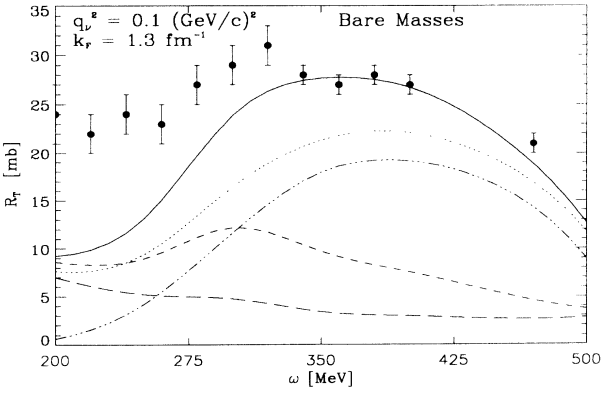

FIG. 18. Results as in Fig. 15, but now for the data of [32] where the four-momentum transfer is kept fixed.

the hadronic medium will give rise to changes of the one-body Green function and to changes of single-nucleon properties. For a finite nucleus these effects will moreover be density dependent and as such a local-density analysis is necessary. In this respect the Fermi gas approximation itself deserves more attention and an analysis with more realistic single-particle wave functions could be preferable. Finally one should worry about unitarity. Simply adding reaction channels may violate probability conservation and give completely wrong results. The fact that in the present treatment there are two channels both showing a resonance behavior strongly suggests that we might be dealing with such a case.

All these effects and considerations are absent in the model that we described up till now. At this point we state that a comparison with the data of a model of the present type is at best qualitatively reliable. A study of several of the shortcomings mentioned above will be the subject of a forthcoming paper [24].

IX. CONCLUSIONS

In this paper we reported on a study of the contribution of relativistic meson exchange and isobar currents to the response of nuclei in electron scattering at intermediate energies in the noninteracting Fermi gas model. We now summarize the conclusions which emerge from this work.

The main result of this work is the apparent importance of the full two-body isobar current in the dip and resonance region due to a resonance behavior. This large qualitative effect is not obtained in the static limit procedure and cannot be found reliably in an approximate way. When we compared the results of the full calculations with the SL ones we found that the quantitative effects generally increase with increasing momentum transfer and become large at the nucleon mass scale.

To be able to make meaningful comparisons with data we studied the real-pion production process in the same framework where we paid special attention to the physical meaning of the Δ-isobar decay width in relation with the isobar model. We showed explicitly that the energy dependence of the decay width effectively accounts for the possible phase space of the produced pion. From this analysis it is clear that a consistent treatment of the $\pi N\Delta$ decay vertex in relation to the Δ-isobar decay width is important, especially in an effective Lagrangian approach. We draw the conclusion that one should be careful to trust results that are obtained in a fixed-width approximation to the Δ-isobar decay width.

Comparison of the results of our model calculations with data are reasonable. The enhancement of the two-body contribution improves the comparison in the dip region considerably. The relativistic model studied in this paper clearly neglects effects of the final-state interactions and the detailed structure of the nucleus. Therefore the above comparisons must be regarded as qualitative. The noninteracting Fermi gas analysis can readily be extended to a more realistic description when we also include the effects of medium modifications. This will be done in a subsequent paper [24].

Finally, at a technical level, our work shows that, given modern computing facilities, there is no reason to resort to static approximations of two-body currents. Furthermore it appeared that a large class of numerical integrations, which result in analyses of the type treated in this paper, can be carried out straightforwardly and without further approximations with the use of Monte Carlo techniques. The amount of work that has been and still is being devoted to approximations in relation to the treatment of the current operator on the one hand and the evaluation of the (Fermi gas) integrals on the other hand makes this a nontrivial conclusion.

ACKNOWLEDGMENTS

This work was supported in part by the Stichting voor Fundamenteel Onderzoek der Materie (FOM), which is sponsored by the Nederlandse Organisatie voor Wetenschappelijk Onderzoek (NWO). Part of the numerical calculations were performed on the Cray YMP of the Amsterdam Computer Centre (SARA), with financial support from the "Stichting Nationale Computer Faciliteiten" (NCF).

APPENDIX A: FORM FACTORS AND COUPLING CONSTANTS

In this appendix we describe the way current conservation is maintained once form factors, both electromagnetic and strong, are taken into account. Moreover, since we want to perform calculations at high ($|\mathbf{q}| > 1$ GeV/c) momentum transfer, our results will be sensitive to details of the phenomenology. For that reason we discuss the choice of form factors and coupling constants in more detail.

For a long time it has been argued that the two-body current, due to the continuity equation, should have the same electromagnetic (EM) form factor as the charge density operator. The latter is phenomenologically well described by the dipole fit:

$$G_E(q^2) = \left(\frac{1}{1 - q^2/\Lambda^2}\right)^2 \tag{A1}$$

with $\Lambda^2 = 0.71$ GeV^2.

If one starts, however, from a microscopic picture there is no other choice than the EM form factor that corresponds to the photon vertex that is contained by the respective diagrams. If one uses current conservation to construct the two-body current in a relativistic framework, like in the work of Hummel and Tjon [34], there is no freedom either. For the π MECs for instance, the nonvanishing isovector commutator gives the isovector form factor $F_1^v = (F_1^p - F_1^n)$ as EM form factor of the two-body current. By fully exploiting the transverse freedom in the construction of the two-body current, Gross and Riska developed a method [35] to extrapolate the current from $q^2 = 0$ to finite q^2, which allows one to use the

correct EM form factor for each diagram.

If strong form factors are to be included, things become even more complicated. Gross and Riska [35] developed a way to guarantee current conservation with the aid of Ward identities, which we apply in our case. The strong form factor is chosen to be given by

$$F_\pi(k^2) = \frac{\Lambda_\pi^2 - m_\pi^2}{\Lambda_\pi^2 - k^2}, \tag{A2}$$

which is normalized to one for a physical pion ($k^2 = m_\pi^2$) [2]. The final result we obtain that way can be written as

$$J^\mu_{\text{in-flight}} = i(\boldsymbol{\tau}_{(1)} \times \boldsymbol{\tau}_{(2)})^3 \left(\frac{g_\pi}{2M}\right)^2 F_{\text{EM}}(q^2) F_\pi(k_1^2) F_\pi(k_2^2)(k_2 - k_1)^\mu (\not{k}_1\gamma^5)_{(1)}(\not{k}_2\gamma^5)_{(2)} \times \left(\frac{1}{(k_1^2 - m_\pi^2)(k_2^2 - m_\pi^2)} + \frac{1}{(k_1^2 - m_\pi^2)(k_1^2 - \Lambda_\pi^2)} + \frac{1}{(k_2^2 - m_\pi^2)(k_2^2 - \Lambda_\pi^2)}\right). \tag{A3}$$

The static limit reduction of this current precisely gives the form of the pion in-flight MEC with the inclusion of strong form factors as given by Mathiot [36]. If one interprets the factor $1/(k^2 - \Lambda_\pi^2)$ as the propagator for a fictitious Λ_π particle, we can view the additional terms appearing in Eq. (A3) as resulting from diagrams where the photon couples to the Λ_π particle.

For the contact terms this procedure gives

$$J^\mu_{\text{contact}} = F_c(q^2) i(\boldsymbol{\tau}_{(1)} \times \boldsymbol{\tau}_{(2)})^3 \left(\frac{g_\pi}{2M}\right)^2 \left[F_\pi^2(k_2^2)\Pi(k_2)_{(2)}(\gamma^\mu\gamma^5)_{(1)} - F_\pi^2(k_1^2)\Pi(k_1)_{(1)}(\gamma^\mu\gamma^5)_{(2)}\right]. \tag{A4}$$

The sum of the currents of Eqs. (A3) and (A4) is the π MEC J^μ_π we use to calculate the meson-exchange contribution of pionic origin to the transverse response.

A phenomenological part of the $\pi N\Delta$-coupling has yet to be discussed. The width as given by Eq. (3.27) does not reproduce the experimental phase shift δ_{33} very well. To improve this, an extra form factor $R(r^2)$ has to be added to the vertices (3.13) and (3.14), depending on the relative πN-momentum r [16,37], which we choose to be:

$$R(r^2) = \left(\frac{\Lambda_R^2}{\Lambda^2 - r^2}\right)^{\frac{1}{2}} \tag{A5}$$

with $r^2 = (E_{\mathbf{k}} - \omega_{\mathbf{k}})^2 - 4\mathbf{k}^2$ and $\Lambda_R^2 = 0.95M^2$. This extra term emerges naturally if the Δ isobar is treated as an interacting πN system, where it is derived from the πN interaction vertex, which is assumed to be of separable form [37]. Form factors depending on the relative three-momentum appear in many other phenomenological works like Moniz [38] and Koch *et al.* [23]. We have chosen its form [16] such that over a large range of energies $\sqrt{s}$ the resulting energy-dependent width compares well with the parametrization of Bransden and Moorhouse [39], which, in turn, gives a good fit to the phase-shift δ_{33}. If one includes it in the isobar current, an ambiguity arises since there the pion is off-shell. We chose to treat it, given the pion three-momentum, as if the pion was on shell, which avoids possible kinematical singularities. The influence of this ambiguity was found to be small when we boosted the momenta from the laboratory to the c.m. frame, applied the above mentioned choice in both frames, and compared the results.

The $\gamma N\Delta$ coupling strength is determined from data for the M_{1+} multipole contribution to pion photoproduction. This makes the determination model dependent and rather large differences appear in the literature. We adopt the original value of Peccei, $f_{\gamma N\Delta} = 5.0$. The q^2 dependence of this coupling (the EM form factor) is experimentally poorly determined. In fact, one essentially only knows that the EM form factor falls off faster with increasing q^2 than the dipole fit to the nucleon form factor, indicating that the Δ-isobar charge radius is larger than that of the proton. Since we want to perform calculations at high ($|\mathbf{q}| > 1$ GeV/c) momentum transfer, our results will be sensitive to details of the phenomenology. For that reason we will discuss these issues in more detail.

To extract the momentum dependence of the coupling constant at the effective Lagrangian level from the experimental data for the M_{1+} multipole, kinematical factors appear due to transitions from one set of invariants to the other [15]. A similar case where this occurs is the transition from Dirac to Sachs form factors of the nucleon. If we follow [15], it appears that we only deal with one of the invariants, which makes the comparison straightforward.

We write the experimentally observable form factor as

$$G_M^*(q^2) = G_{\text{dipole}}(q^2)\, G_{\text{extra}}(q^2)\, G_M(0) \tag{A6}$$

(for $q^2 = 0$ we normalize all form factors to 1) and we have the kinematical transformation [15,22]

$$G_M^*(q^2) = \frac{M(3M_\Delta + M)}{3M_\Delta}\left(1 - \frac{q^2}{\Lambda_1^2}\right)\left(1 - \frac{q^2}{\Lambda_2^2}\right)^{-\frac{1}{2}} \times \frac{f_{\gamma N\Delta}}{2M} F_{\gamma N\Delta}(q^2) \tag{A7}$$

[2] Typical values for the cutoff Λ_π^2 in one-boson-exchange (OBE) models range from 1 to 2 GeV^2. The value we adopted was taken from Van Faassen [18], which was determined in a one-boson-exchange model which included the Δ isobar. The value is given by $\Lambda_\pi^2 = 1.9M^2$.

with $\Lambda_1^2 = (3M_\Delta + M)(M_\Delta + M)$ and $\Lambda_2^2 = (M_\Delta + M)^2$. Combining these expressions, using the compilation of data for $G_M^*(q^2)$ from [22], we find, with $G_M^*(0) = 3.0$:

$$f_{\gamma N\Delta} = 4.8 \quad \text{and}$$

$$F_{\gamma N\Delta}(q^2) = G_{\text{dipole}}(q^2)\left(1 - \frac{q^2}{\Lambda_2^2}\right)^{-\frac{1}{2}}\left(1 - \frac{q^2}{\Lambda_3^2}\right)^{-\frac{1}{2}} \tag{A8}$$

with $\Lambda_3^2 = 3.5\ \text{GeV}^2$. Note that this value for $f_{\gamma N\Delta}$ differs only slightly from the one of Peccei.

Finally we have to address the strong form factor at the $\pi N\Delta$ vertex. For this we take the parametrization in the one-boson-exchange model with Δ degrees of freedom as given by Van Faassen:

$$F_{\pi N\Delta}(k^2) = \frac{\Lambda_{\pi N\Delta}^2}{\Lambda_{\pi N\Delta}^2 - k^2}. \tag{A9}$$

This term is included at each $\pi N\Delta$ vertex. The cutoff value $\Lambda_{\pi N\Delta}$ is given by

$$\Lambda_{\pi N\Delta}^2 = 1.5M^2.$$

We emphasize that the present form factor regularizes the $\pi N\Delta$ vertex once the pion is far off-shell and therefore has a different role compared with the previous one of Eq. (A5), which is already important when the pion is on-shell.

APPENDIX B: PAULI EXCHANGE CONTRIBUTION TO $W^{\mu\nu}$

In this appendix we derive the Pauli exchange part of the two-particle–two-hole (2p2h) contribution to $W^{\mu\nu}$. As mentioned in Sec. IV this is most easily done in the second-quantization approach and will be demonstrated below.

In the second-quantization approach, the 2p2h state is written as

$$|\text{2p2h}\rangle = a_{p_2'}^\dagger a_{p_1'}^\dagger a_{p_1} a_{p_2}|\text{FG}\rangle, \tag{B1}$$

where $|\text{FG}\rangle$ denotes the Fermi gas ground state, and a_p and $a_p^\dagger$ the usual annihilation and creation operators, respectively. To shorten notation, p_i is understood to represent both the momentum $\mathbf{p}_i$ and the spin and isospin quantum numbers s_i and t_i of the one-particle state. The two-body (2p2h) current is given by

$$J^\mu = \tfrac{1}{2}\sum_{k_1\ldots k_2'} \tilde{J}^\mu(k_1,k_2,k_1',k_2')a_{k_2'}^\dagger a_{k_1'}^\dagger a_{k_1} a_{k_2} \times\theta^<(\mathbf{k}_1)\theta^<(\mathbf{k}_2)\theta^>(\mathbf{k}_1')\theta^>(\mathbf{k}_2') \tag{B2}$$

with

$$\tilde{J}^\mu(k_1,k_2,k_1',k_2') = \bar{u}_{(2)}(k_2')\bar{u}_{(1)}(k_1')\hat{J}^\mu u_{(1)}(k_1)u_{(2)}(k_2).$$

Normal ordering we then find

$$\langle\text{2p2h}|J^\mu|\text{FG}\rangle = \left(\tilde{J}^\mu(p_1,p_2,p_1',p_2') - \tilde{J}^\mu(p_1,p_2,p_2',p_1')\right) \times\theta^<(\mathbf{p}_1)\theta^<(\mathbf{p}_2)\theta^>(\mathbf{p}_1')\theta^>(\mathbf{p}_2') \tag{B3}$$

and

$$\langle\text{2p2h}|J^\nu|\text{FG}\rangle^* = \left(\tilde{J}^{*\nu}(p_1,p_2,p_1',p_2') - \tilde{J}^{*\nu}(p_1,p_2,p_2',p_1')\right) \times\theta^<(\mathbf{p}_1)\theta^<(\mathbf{p}_2)\theta^>(\mathbf{p}_1')\theta^>(\mathbf{p}_2') \tag{B4}$$

with

$$\tilde{J}^{*\nu}(p_1,p_2,p_1',p_2') = \bar{u}_{(2)}(p_2)\bar{u}_{(1)}(p_1)\bar{J}^\nu u_{(1)}(p_1')u_{(2)}(p_2')$$

where one must use the Dirac adjoint $\bar{J}^\nu = \gamma_{(1)}^0\gamma_{(2)}^0\hat{J}^\nu\gamma_{(1)}^0\gamma_{(2)}^0$. The labels (1) and (2) represent the particle labels. The first term in Eq. (B3) is the direct, the second the exchange matrix element. Using the expression in Eq. (2.4) for $W^{\mu\nu}$ we thus have

$$W^{\mu\nu} = \tfrac{1}{4}2(2\pi)^3 V\sum_{p_1\cdots p_2'}\bar{u}_{(1)}(p_1)\bar{u}_{(2)}(p_2)\bar{J}^\nu u_{(2)}(p_2')u_{(1)}(p_1')[\bar{u}_{(2)}(p_2')\bar{u}_{(1)}(p_1') - \bar{u}_{(1)}(p_2')\bar{u}_{(2)}(p_1')]\hat{J}^\mu u_{(1)}(p_1)u_{(2)}(p_2)$$
$$\times\theta^<(\mathbf{p}_1)\theta^<(\mathbf{p}_2)\theta^>(\mathbf{p}_1')\theta^>(\mathbf{p}_2')\delta^4(p_1+p_2+q-p_1'-p_2'), \tag{B5}$$

where the factor 2 is obtained from the equivalence of terms after renaming the (dummy) particle labels and the factor $\frac{1}{4}$ accounts for the double counting of identical particle-hole pairs. For the first term in Eq. (B5) we obtain, carrying out the spin summations, the result of Eq. (4.6). The second, Pauli-exchange, term has the difficulty that the indices are "at the wrong place" in the expression:

$$P_e(\mathbf{p}_1',\mathbf{p}_2') = (2M)^2\sum_{s_1's_2'}u_{(2)}(p_2')u_{(1)}(p_1')\bar{u}_{(1)}(p_2')\bar{u}_{(2)}(p_1'), \tag{B6}$$

where the factor $(2M)^2$ has been chosen such that this operator equals the operator in Eq. (4.8). One commonly used technique to treat this is the application of a Fierz

transformation, which amounts to an effective transformation of the current operator. Since this is hard to implement in the present case, we choose to explicitly carry out the spin summations in the operator of Eq. (B6). This is most easily done if we replace the spinors in Eq. (B6) with the aid of

$$u(\mathbf{p},s)=\frac{\hat{\not{p}}+M}{\sqrt{2M(E_{\mathbf{p}}+M)}}u(0,s)$$

and then explicitly construct the 4×4 matrices for these zero-momentum spinors and subsequently write them in terms of γ matrices. We then obtain

$$P_{\rm e}(0,0)=(2M)^2\sum_{s_1's_2'}u_{(2)}(0,s_2')u_{(1)}(0,s_1')\bar{u}_{(1)}(0,s_2')\bar{u}_{(2)}(0,s_1')=\tfrac{1}{2}(I_{(1,2)}+\sigma^{ij}_{(1)}\sigma^{(2)}_{ij})\tfrac{1}{2}(I+\gamma^0)_{(1)}\tfrac{1}{2}(I+\gamma^0)_{(2)} \quad \text{(B7)}$$

and

$$P_e(\mathbf{p}_1',\mathbf{p}_2')=\frac{1}{(E_{\mathbf{p}_1'}+M)(E_{\mathbf{p}_2'}+M)}\Lambda^+_{(1)}(\mathbf{p}_1')\Lambda^+_{(2)}(\mathbf{p}_2')P_e(0,0)\Lambda^+_{(1)}(\mathbf{p}_2')\Lambda^+_{(2)}(\mathbf{p}_1') \quad \text{(B8)}$$

with $\Lambda^+(\mathbf{p})$ the usual positive-energy projection operators. Since this expression for P_e is given completely in terms of four-vectors and γ matrices, it is suited to be evaluated with the same techniques (i.e., with the aid of FORM) as the direct term and we can incorporate it in our evaluations of the response functions.

[1] *Modern Topics in Electron Scattering*, edited by B. Frois and I. Sick (World Scientific, Singapore, 1991).
[2] M.J. Dekker, P.J. Brussaard, and J.A. Tjon, Phys. Lett. B **266**, 249 (1991).
[3] M.J. Dekker, P.J. Brussaard, and J.A. Tjon, Phys. Lett. B **289**, 255 (1992).
[4] P. Barreau *et al.*, Nucl. Phys. **A402**, 515 (1983).
[5] Z.E. Meziani *et al.*, Phys. Rev. Lett. **54**, 1233 (1985).
[6] M. Bernheim *et al.*, Phys. Rev. Lett. **46**, 402 (1981).
[7] J.W. Van Orden, T.W. Donnelly, T. de Forest Jr., and W.C. Hermans, Phys. Lett. **B76**, 393 (1978).
[8] J.W. Van Orden and T.W. Donnelly, Ann. Phys. (N.Y.) **131**, 451 (1981); J.W. Van Orden, Ph.D. thesis, Stanford University (unpublished).
[9] J.D. Björken and S.D. Drell, *Relativistic Quantum Fields* (McGraw-Hill, New York, 1964).
[10] J.P. Chen *et al.*, Phys. Rev. Lett. **66**, 1283 (1991).
[11] G.B. West, Phys. Rep. **18**, 263 (1975).
[12] R.D. Peccei, Phys. Rev. **176**, 1812 (1968); *ibid.* **181**, 1902 (1969).
[13] M. Bénmerrouche, R.M. Davidson, and N. Mukhopadhai, Phys. Rev. C **39**, 2339 (1989).
[14] M. Veltman, in *Weak Interactions and High-Energy Neutrino Physics, International School of Physics Enrico Fermi, course XXXII*, 1964, edited by T.D. Lee (Academic, New York, 1966).
[15] H.F. Jones and M.D. Scadron, Ann. Phys. (N.Y.) **81**, 1 (1973).
[16] E. van Faassen, Ph.D. thesis, University of Utrecht (unpublished).
[17] J. Vermaseren, FORM, an algebraic manipulation program for large formulae (NIKHEF-H, Amsterdam, The Netherlands).
[18] E. van Faassen and J.A. Tjon, Phys. Rev. C **30**, 285 (1984).
[19] J. Hockert, D.O. Riska, M. Gari, and A. Huffman, Nucl. Phys. **A217**, 14 (1973).
[20] I.S. Towner, Phys. Rep. **155**, 263 (1987).
[21] T. Ericson and W. Weise, *Pions and Nuclei* (Oxford University, New York, 1988).
[22] E. Amaldi, S. Fubini, and G. Furlan, *Springer Tracts in Modern Physics* (Springer, Berlin, 1979), Vol. 83.
[23] J.H. Koch and N. Ohtsuka, Nucl. Phys. **A435**, 765 (1985).
[24] M.J. Dekker, P.J. Brussaard, and J.A. Tjon, in preparation.
[25] K. Wehrberger and F. Beck, Phys. Lett. B **270**, 1 (1991).
[26] K. Wehrberger, C. Bedau, and F. Beck, Nucl. Phys. **A504**, 797 (1989).
[27] E. Rost, C.E. Price, and J.R. Shepard, Phys. Rev. C **47**, 2250 (1993).
[28] M.J. Dekker, Ph. D. thesis, University of Utrecht (unpublished).
[29] E.J. Moniz, Phys. Rev. **184**, 1154 (1969).
[30] M. Gari and W. Krümpelmann, Z. Phys. A **322**, 689 (1985).
[31] T. Takaki, Phys. Rev. Lett. **62**, 395 (1989); Phys. Rev. C **39**, 359 (1989).
[32] D.T. Baran *et al.*, Phys. Rev. Lett. **61**, 400 (1988).
[33] C.R. Chinn, A. Picklesimer, and J.W. van Orden, Phys. Rev. C **40**, 790 (1989).
[34] E. Hummel and J.A. Tjon, Phys. Rev. C **42**, 423 (1990).
[35] F. Gross and D.O. Riska, Phys. Rev. C **36**, 1928 (1987).
[36] J.-F. Mathiot, Phys. Rep. **173**, 63 (1989).
[37] W.M. Kloet and J.A. Tjon, Phys. Rev. C **30**, 1653 (1984).
[38] E.J. Moniz and A. Sevgen, Phys. Rev. C **24**, 224 (1981).
[39] B.H. Bransden and R.G. Moorhouse, *The Pion Nucleon System* (Princeton University, Princeton, 1973).